DESIGN AND ANALYSIS OF NANO VIBRATORY BEAM GYROSOPE

A thesis submitted in the partial fulfilment

of the requirement for the degree of

Master of Technology

in

Mechanical Engineering

(Specialization: - Machine Design and Analysis)

Submitted by

Ashish Kumar Gurjar

(Roll No: - 213ME1378)

DEPARTMENT OF MECHANICAL ENGINEERING

NATIONAL INSTITUTE OF TECHNOLOGY

ROURKELA- 769008, ODISHA, INDIA

JUNE 2015

DESIGN AND ANALYSIS OF NANO VIBRATORY BEAM GYROSOPE

A thesis submitted in the partial fulfilment

of the requirement for the degree of

Master of Technology

in

Mechanical Engineering

(Specialization: - Machine Design and Analysis)

Submitted by

Ashish Kumar Gurjar

(Roll No: - 213ME1378)

Under the supervision of

Prof. J. Srinivas

DEPARTMENT OF MECHANICAL ENGINEERING

NATIONAL INSTITUTE OF TECHNOLOGY

ROURKELA- 769008, ODISHA, INDIA

JUNE 2015

DEPARTMENT OF MECHANICAL ENGINEERING

NATIONAL INSTITUTE OF TECHNOLOGY

ROURKELA- 769008, ODISHA, INDIA

CERTIFICATE

This is to certify that the thesis entitled **"DESIGN AND ANALYSIS OF NANO VIBRATORY BEAM GYROSCOPE"** submitted by '**Ashish Kumar Gurjar**' to the **National Institute of Technology (NIT), Rourkela** for the award of **Master of Technology** in **Machine Design and Analysis**, is a record of bonafide research work carried out by him in the **Department of Mechanical Engineering**, under the supervision and guidance.

I believe that this thesis fulfils part of the requirements for the award of degree of Master of Technology. The results embodied in the thesis have not been submitted for the award of any other degree elsewhere.

Place: - Rourkela

Date: -

Prof. J. Srinivas

Department of Mechanical Engineering

National Institute of Technology

Rourkela- 769008

ACKNOWLEDGEMENT

My first thanks are to the Almighty God. I am extremely fortunate to be involved in an exciting and challenging research project work on "**Design and analysis of nano vibratory beam gyroscope**". I would like to express my greatest gratitude to my supervisor **Prof. J. Srinivas**, for his excellent guidance, valuable suggestions and endless support. He has not only been a wonderful supervisor but also an honest and sincere person. I consider myself extremely lucky to be able to work under guidance of such a dynamic personality. He is one of such genuine person for whom my words will not be enough to express.

I would like to express my sincere thanks to Prabhu L, K. V. Varalakshmi, Sk. Jakeer Hussain, Puneet Kumar and all my classmates for their precious suggestions and encouragement to perform the project work. I am very much thankful to them for giving their valuable time for me.

Finally, I express my sincere gratitude to my parents for their constant encouragement and support at all phases of my life.

ASHISH KUMAR GURJAR

ABSTRACT

Gyroscope is an angular rate measurement sensor having broad application in the field of automotive, military services, aerospace and consumer electronics industries. Silicon micro machined MEMS vibratory gyroscopes have better advantages compared to conventional gyroscope. Nano beam vibratory gyroscope is one of the simple gyroscope. It has relatively small size, light weight, low power consumption, low cost and simple structure. When a gyroscope is made to rotate at its base along with some excitation in one of the bending direction, due to Coriolis effect, there will be significant displacement in other bending direction. Dynamic modeling of beam gyroscope is very interesting area. In the micro/nano level actuation and sensing are with electrostatics principles. This report presents the modeling and analytical simulation task of a nano cantilever beam gyroscope. Static and dynamic analysis of a nano/micro cantilever gyroscope with a tip mass is studied. Pull-in instability corresponding voltage is estimated from static and frequency response. Pull-in stability regions are identified as a function of beam length, tip mass value, elastic modulus of the beam. Nonlinearities due to geometry and the external forces including electrostatic and van der Waals forces are considered during modelling. Squeeze film and slide film damping are considered to account the damping force between the tip mass and sense and drive direction. The dynamic solution is obtained by using Galerkin's reduction scheme. The time response and the frequency domain graphs are arrived for different parameters on both sense and drive directions. The interactive program developed in the work are helpful to account any experiments for additional force at nano level.

CONTENTS

LIST OF FIGURES

LIST OF TABLES

Nomenclature

L	Length of the beam (μm)
b	Width of the beam (μm)
h	Thickness of the beam (μm)
Ω	Base rotation (rad/sec)
J	Polar moment of inertia of the beam (μm^4)
m	Mass per unit length of the beam (kg/m)
M	Tip mass (kg)
V_{DC}	DC voltage (V)
V_{AC}	AC voltage (V)
d_v	Initial gap between sense electrode and tip mass (μm)
d_w	Initial gap between drive electrode and tip mass (μm)
ρ	Density of the beam and tip mass material (kg/m^3)
A	Cross-sectional area of the beam (m^2)
ε	Electrical permittivity
E	Young's modulus (Gpa)
I	Moment of inertia of the beam cross-sectional
A_v	Area of sense electrode
A_w	Area of drive electrode
F_c	Casimir forces per unit area
h	Planck's constant
c	Speed of light (m/sec)
h_g	Distance between the plates

F_{1c}	Casimir force in drive direction
F_{2c}	Casimir force in drive direction
F_{vdW}	Vander waal force per unit area
H	Hamaker coefficients
F_{1vdW}	Vander waal force in drive direction
F_{2vdW}	Vander waal force in sense direction
υ	Poisson's ratio
G	Shear modulus
μ	Gas viscosity (Pa s)
μ_{SL}	Effective gas viscosity for slide film damping
K_n	Knudsen number
λ	Gas mean free path (m)
P	Gas pressure (Pa)
C_{SL}	Slide film damping coefficients
μ_{SQ}	Effective gas viscosity for squeeze film damping
C_{SQ}	Squeeze film damping coefficients

CHAPTER 1
INTRODUCTION

Micromachined angular rate gyroscopes are often finding applications in several systems including aviation, consumer electronics and defence sectors. Various MEMS gyroscopes are being recently developed and implemented in various applications. Design and analysis, fabrication and electronic circuitry are typical issues in development of MEMS/NEMS gyroscope. Vibratory MEMS gyroscopes convert the mechanical displacements into equivalent electrical voltage in sense direction. Conversion efficiency (sensitivity), operating range, accuracy of measurements (resolution) are ultimate parameters for gyroscope designation. Tuning fork type, beam type and ring type are few commonly used vibratory gyroscopes.

Gyroscope first discovered in 1817, by Johann Bohnenberger. Gyroscopes are the angular rate sensors which can be used for measuring or maintaining orientation from the principles of angular momentum. The device is having a disk or wheel and an inner gimbal and an outer gimbal as shown in Fig. 1.1.

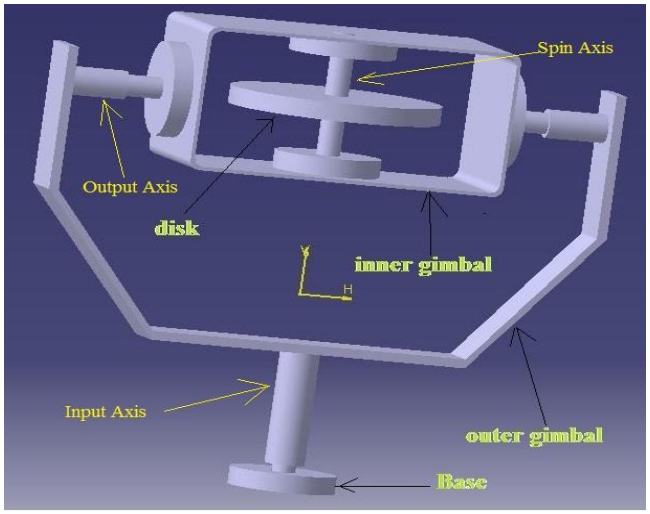

Fig. 1.1 Traditional Gyroscope

The axle of disk is free to take any of the orientation. The gimbals are used to minimize the external torque. Traditional gyroscope having a disk which is rotating along the direction of the engine shaft. The axis of rotation of the disk is called spin axis. Rotating disk is surrounded by an inner gimbal. Inner gimbal can also rotate about its axis. The axis of inner gimbal is perpendicular to the spin axis and inner gimbal is covered by an outer gimbal whose axis is perpendicular to inner gimbal axis. The spin axis, inner gimbal axis and outer gimbal axis are mutually perpendicular to each other. One of inner or outer gimbal axis represents the input axis and other one as output axis. When a small disturbances comes in input axis then the combined effect of spinning and disturbance will observed in output axis which is known as gyroscopic effect. The output axis also known as precession axis.

1.1 Micro-Gyroscopes

One of the important MEMS sensors is a micro-gyroscope. Conventional gyroscopes are heavy, costly and bulky. Micro-gyroscopes solve these problems and can be employed in highly sensitive applications for measurement of rotation rate. These gyroscopes have various properties such as durability, light weight, low energy consumption, small dimension and low cost. Now-a-days ample amount of research works are carried out in the field of micro-gyroscope in all over the world. Microfabrication technology is used to construct the MEMS gyroscope. Several materials are used for manufacturing of micro-gyroscope but out of which silicon is very famous choice for fabrication of micro-gyroscopes, because it can be used as a single crystal substrate. The physical properties of silicon made it more suitable for micromachining. Micro gyroscopes can also be integrated easily with microelectronics. The MEMS gyroscopes are classified based on various mechanisms of sensing. Most of these employ vibration principles and use Coriolis force to

measure angular displacement. Examples of vibratory gyroscopes include tuning fork gyroscope, ring gyroscope and vibratory beam type gyroscope.

In 1990s the first tuning fork gyroscope made by draper laboratory. The tuning fork gyroscope is relatively easy to fabricate and having high precision performance. The tuning fork gyroscope is work on Coriolis Effect. The tuning fork gyroscope having two oscillating frames, both the frame supported by glass substrate by using four spring type beams and these frames are connected by a connection ring. The proof masses along with electrodes are connected to frames with the help of two suspension beams. The frames and the proof masses can move above the glass substrate along the plane in x and y axis direction. The Ac current supply in the drive direction due to this Lorentz force field is generated in x direction, which create vibration in the oscillating frame. When the rotation is given about the z-direction then due to Coriolis effect the proof masses move along y axis. This vibration in y axis sensed by capacitive sensor. According to connection the tuning fork gyroscopes are two type, direct connection mode and indirect connection mode. Indirect connection type tuning fork gyroscope is accurate compare to direct type connection tuning fork gyroscope. Tuning fork gyroscope is very useful in automobile application. Fig. 1.2 shows the tuning fork gyroscope.

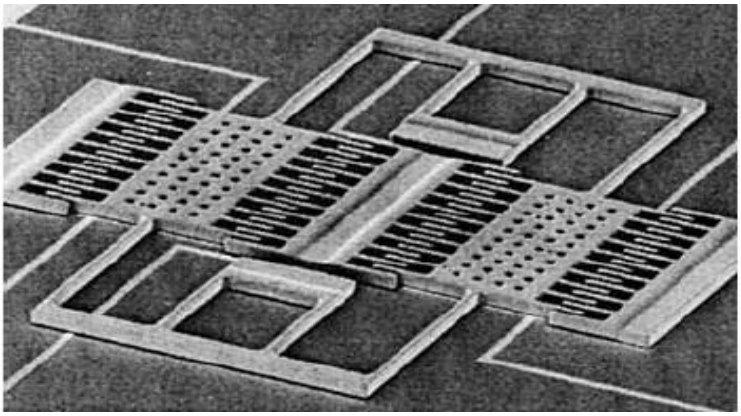

Fig. 1.2 Tuning fork gyroscope [21]

Vibratory ring type gyroscope is first developed by the researcher of Michigan University. Vibratory ring type gyroscope consist of a semi-circular support spring, vibrating ring, control, sense and drive electrode. The vibratory ring gyroscopes are fabricated by using high aspect ratio combined poly and single crystal MEMS technology. Vibrating ring is symmetric in nature, so eight spring placed in 45^0 apart from each other is used to support and balancing purposes. Each spring has two electrode one for driving and one for sensing purpose. The electrostatic force provide vibration in an in-plane elliptically shaped primary flexural mode with constant amplitude. When the ring is rotate about its normal axis then the primary vibration transferred to secondary mode and it is sensed by sense electrode. Fig. 1.3 represents the vibratory ring type gyroscope.

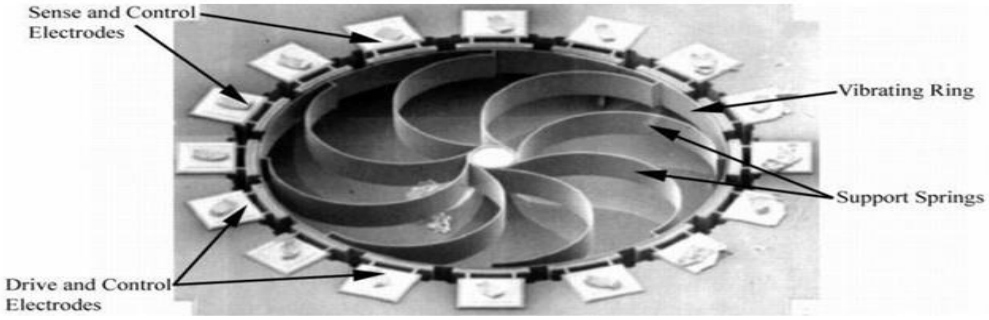

Fig. 1.3 Vibratory ring type gyroscope [22]

Vibratory beam type gyroscope is a type of MEMS device, which is having a cantilever beam fixed at one end and a small tip mass attached to its other end. The beam is rotate about the x-axis, called spin axis and having two bending direction. The beam is actuated in z-direction by using electrostatic actuation technique with the help of drive electrode. Due to this actuation and base rotation the secondary vibration generated in the y-direction and a sense electrode is used to sense the deflection due to secondary vibration. The control algorithm is generated to study the gyroscopic effect and this gyroscope used as a sensor for the various application. In all above type,

the architecture should generate and maintain a constant linear or angular momentum coupled to the sense mode.

1.2 Literature Review

Due to their advantages, such as simplicity and easy to fabricate from micro fabrication techniques, several recent works focused on beam-type gyroscopes

First beam gyroscope was demonstrated in early 1983 by Shupe and Connor [1] using electrostatic force as excitation with a frequency close to cantilever frequency and piezoelectric element was used for sensing induced vibration.

Tanaka et al [2] fabricated a vibratory micro-gyroscope by using silicon. They used silicon surface micromachining process for fabrication. Electrostatic actuation is used for drive the gyroscope and capacitive sensing adopted for sensing purpose.

Maenaka et al. [3] investigate the behaviour of the micro-gyroscope by considering beam as a vibrating mass.

Katz and Highsmith [4] studied about the optimal size of the vibratory beam type gyroscope because the thermal noise is depend upon the beam length. They concluded that for longer beam the thermal noise is lower. These work very helpful for the application of gyroscope in aviation because noise play important role for the development of aviation vehicles.

Yang and Fang [5] performed the vibration study of elastic beam having piezoelectric surface bonded films and rotating about one of its axis. They also considered the effect of centripetal force and Coriolis forces. They proposed a beam model can be used for gyroscope.

Kausinis and Barauskas [6] represented the 3 dimension finite element analysis model of a piezoelectric angular rate sensor for estimating the dynamic properties. For achieving the desired

values of natural frequencies they adjust the geometric parameter and obtained the sensitivity functions.

Yu et al. [7] constructed thin and short cantilevers having high resonance frequency and low force constant.

Seok and Scarton [8] studied the dynamic characteristics of a beam type angular rate gyroscopic sensor. They considered the square cross-section of the vibratory beam and performed the sensitivity and bandwidth analysis of these beam. They concluded that by increasing the bandwidth of the sensor the sensitivity decreases.

Esmaeili et al. [9] study the performance and dynamic modelling of a vibratory beam type gyroscope by considering general support motion. They considered that the beam vibrate in all 3 direction and the beam is rotate about longitudinal direction. Equation of motion are derived by using Extended Hamilton Principle. They considered the effect of Coriolis accelerations, angular accelerations, and beam distributed mass, centripetal accelerations and tip mass on the performance of gyroscope.

Ashokanthan and Cho [10] investigated the dynamic stability of beam type gyroscope under the rate fluctuations. For fluctuations in velocity of rotating beam type gyroscope a mathematical model is developed. The system is having gyroscopic coupling so due to these gyroscopic coupling the variation in natural frequency are characterized. The dynamic stability is investigated due to variation in input angular speed. Numerical integration technique is used to validate the results.

Bhadbhade et al. [11] studied about the vibrating beam type gyroscope which is having a cantilever beam fixed at one end and a tip mass is attached to its other end and it is piezo-electrically actuated. Extended Hamilton principle used for mathematical modelling of the system. Results shows that the performance of gyroscope is depend upon the secondary base rotation of the beam. They also

concluded that with increase in beam length, primary excitation amplitude and base rotation rate the gyroscopic effect will increase.

Ghommem et al. [12] developed a model of the micro beam type gyroscope whose principal component are a micro cantilever beam which is fixed at one end and an small proof mass is attached to its other end. The beam having flexural vibration in two perpendicular axis due to bending and these two modes are coupled by a base rotation. They consider one bending direction as a sense direction and other as a drive direction. Initially the beam is rotated along the longitudinal axis and a pair of DC and AC voltage is applied in the drive direction which is also called electrostatic actuation. Due to these actuation and base rotation the deflection occurs in the third perpendicular direction. The response of those deflection is measured with the help of sense electrode which is assembled in the sense direction. Due to those combined effect the equation of motion for two orthogonal bending direction are derived by using extended Hamilton principal. These equation of motion are solved analytically and the response of the DC voltage and excitation frequency examined.

Hou et al. [13] studied the effect of axial force on the performance of the vibratory gyroscope. They concluded that if material of substrate and structure are having different properties so due to mismatching between the thermal coefficients of expansion the thermal stress induced the axial force. They obtained the effect of axial force on the resonant frequency analytically.

Rasekh et al. [14] studied about the performance of vibratory beam gyroscope having high operational frequency. In this study electrostatic actuation and capacitive sensing are used for driving and sensing respectively. The complete dynamic equation is derived by extended Hamilton principal. Performance of gyroscope like dynamic response, rate sensitivity, resolution, band

width, dynamic range, gyroscope sensitivity and shock resistance are investigated through the simulation results.

Lajimi et al. [15] studied the static and dynamic behaviour of the micro cantilever beam type gyroscope. They investigated the sensitivity of the gyroscope and the parameter which affect the response of the gyroscope.

Lajimi et al. [16] performed the eigenvalue analysis of the vibratory beam type gyroscope and result the variation between frequencies and input angular rate. For these analysis they obtained the characteristic equation and solved for natural frequency. They found that frequencies vary proportionally with the input angular displacements.

Wang et al. [17] shown the design of micromachined gyroscope with multi degree of freedom and double sense mode.

Moghaddam et al. [18] studied about the parameters which are affecting the fundamental frequency and pull-in voltage for the micro cantilever beam type vibratory gyroscope.

Mojahedi et al. [19] investigated the effect of the intermolecular forces on the pull-in instability and the static deflection of the nano/micro vibratory cantilever type gyroscope having a tip mass at its other end. They also studied the non-linearity's due to inertial and geometry terms. They consider Van der Waals and Casimir forces along with electrostatic forces. They used Galerkins technique and Homotopy perturbation method for solution of non-linear equilibrium equation. The effect on pull-in instability due to different parameter are investigated and the response of DC voltages across the drive and sense direction is obtained.

Zand and Moghaddam [20] presented the effect of design parameters on pull-in voltage and fundamental frequency of an electrostatically actuated beam micro-gyroscope.

1.3 Scope and objective of the Work

Few works have considered the effects of damping or influence of intermolecular forces but none of these considered the combined effect of damping and intermolecular forces on the gyroscopic performance. The present work considers a nano-cantilever vibratory beam gyroscope with a tip mass actuated electrostatically and sensed. The influence of the intermolecular forces on the static and dynamic analysis is also considered. Objective of the presents work as follows:

i. Mathematical modelling of the beam type gyroscope and derive the general equation of motion for the system.
ii. Static analysis task by eliminating the time coordinate from the equation and considering the effect of intermolecular force.
iii. Modal and vibration analysis of the cantilever beam having tip mass at its end.
iv. Reduction of 4^{th} order partial differential equation into 2^{nd} order ordinary differential equation by using Galerkin's technique and solve the equations by R-K method.
v. Dynamic analysis of the beam by considering the effect of inter molecular forces and damping forces.
vi. Construct the lumped parameter model for the system to get dynamic response.

The thesis is organized in the following format:

Chapter 2, consist of mathematical modelling of the vibratory beam gyroscope, static uncoupled equation, and introduction of intermolecular forces. Galerkin's method and dynamic coupled equation and damping formulae along with FEA modelling and lumped parameter model also discussed.

Chapter 3 and chapter 4 results and discussion and conclusions respectively

-------o------

CHAPTER 2

MATHEMATICAL MODELLING

Beam is the distribute parameter system with two bending displacement. When such a system is made to rotate at its base along with some excitation in one of the bending direction, due to Coriolis Effect there will be significant displacement in other bending direction. This chapter presents dynamic equations of motion of beam gyroscope in lumped parameter spring mass form, distributed continuous system form and also numerical finite element form. The solution of these equations are shown as static, frequency and dynamic analysis outputs. Approximate and numerical techniques are used to solve the differential equations.

2.1 Type of Actuation Technique used in MEMS gyroscope

Actuation techniques are very important for design and development of micro gyroscope. There are many actuation technique used for analysis point of view of micro and nano gyroscope, but electrostatic actuation, magnetic and piezoelectric actuations are the conventional method which are generally used for micro gyroscope. Due to high current density and ease of control the electrostatic actuation technique is most widely used actuation technique now a days. In this work electrostatic technique is used for both driving and sensing purpose.

In electrostatic technique two conductors are used. Voltage is supplied between these conductors so due to potential difference the electric field is generated by the charge particle. The electrostatic field applied by the generated electric field. The force expression can be derived by differentiating the energy stored per unit length in the capacitor with respect to gap between the conductors. The electrostatic force is inversely proportional to the square of the gap between the conductors so this

is the main problem of electrostatic actuation but in microscopic scale it is beneficial because the micro structures has low aspect ratio and the gap between the conductor also very small. In the design of MEMS system this is the most widely used technique compare to other one. It is also used in accelerometer, switches, micro resonators and micro mirrors etc. Fig. 2.1 shows the electrostatic actuation technique.

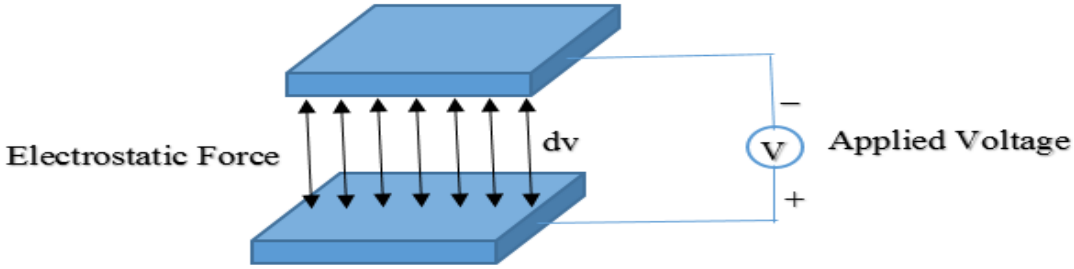

Fig 2.1 Electrostatic actuation

2.2 General equation of motion

The beam type gyroscope is shown in the fig.2.2. The gyroscope having a cantilever beam which is fixed at one end and proof mass is attached to its other end. The beam has uniform cross-sectional area, length L and the m is the mass per unit length of beam. The beam is having two bending direction and the deflection in these direction are v(x, t) and w(x, t) in y and z direction respectively. The beam is rotating along the x axis hence these bending deflection are coupled by a base rotation. The expression for kinetic energy is written as follows:

$$K.E. = \frac{1}{2}\int_0^L [2\Omega^2 J(v'^2 + w'^2) + m(\dot{v}^2 + \dot{w}^2)]dx + \frac{1}{2}\int_0^L m[2(v\dot{w} - w\dot{v})\Omega + \Omega^2(v^2 + w^2)]dx$$

$$+\frac{1}{2}\int_0^L [J\dot{v}'^2 + J\dot{w}'^2 + 2\Omega J(v'\dot{w}' + w'\dot{v}')]dx + \frac{M}{2}(\dot{v}_L^2 + \dot{w}_L^2 + 2v_L\dot{w}_L\Omega - 2w_L\dot{v}_L\Omega + v_L^2\Omega^2 + w_L^2\Omega^2) + LJ\Omega^2$$

(2.1)

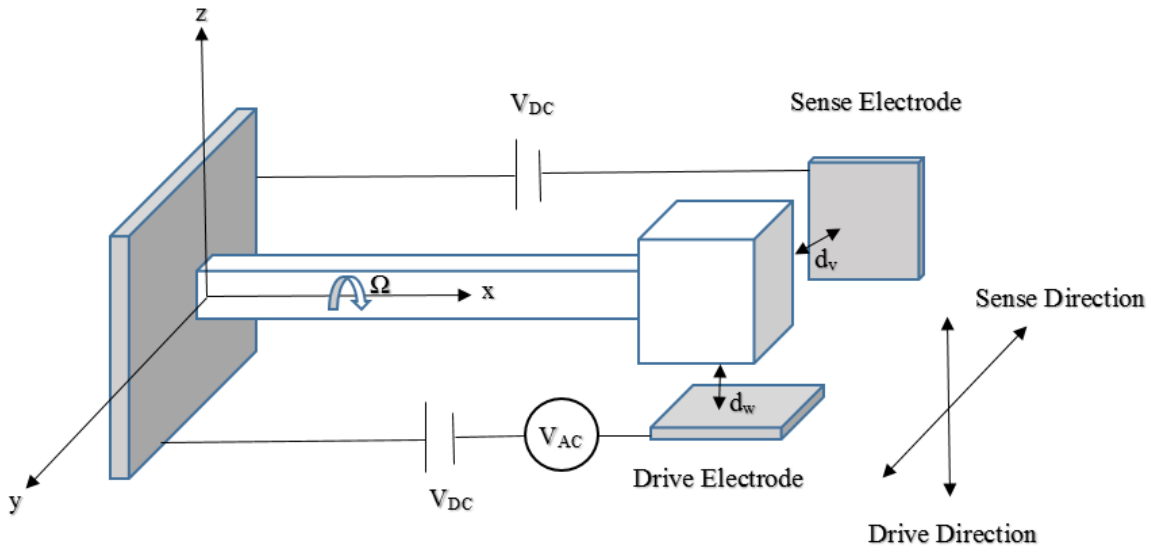

Fig. 2.2 Cantilever beam having rotation about longitudinal axis

Where,

$$J = \int_A \rho y^2 dA = \int_A \rho z^2 dA \tag{2.2a}$$

$$m = \rho A, v_L = v(L,t), w_L = w(L,t) \tag{2.2b}$$

Here dot and prime represents derivatives with respect to time, t and x respectively.

Similarly the expression for the potential energy can be written as follows for the beam gyroscope subjected to electrostatic force in sense and drive direction.

$$P.E. = \frac{1}{2} EI \int_0^L (v''^2 + w''^2) dx - \frac{\varepsilon A_v V_{DC}^2}{2(d_v - v_L)} - \frac{\varepsilon A_w (V_{DC} + V_{AC}(t))^2}{2(d_w - w_L)} \tag{2.3}$$

Where,

A_v= area of sense electrode

d_v=initial gap between tip mass and sense electrode

A_w=area of drive electrode

d_w=initial gap between tip mass and drive electrode

Hamilton principle can be used for deriving the governing equation of motion for the flexural vibration of the system.

$$\int_{t_1}^{t_2}[\delta(K.E.)-\delta(P.E.)]dt=0 \tag{2.4}$$

The equation of motion for the two bending direction is as follows after using the Hamilton principle.

$$EIv^{iv}-mv\Omega^2+2Jv''\Omega^2-2mw\dot{\Omega}+m\ddot{v}-mw\dot{\Omega}-\dot{\Omega}Jw''-J\ddot{v}''=0 \tag{2.5}$$

$$EIw^{iv}-mw\Omega^2+2Jw''\Omega+2mv\dot{\Omega}+m\ddot{w}+mv\dot{\Omega}-\dot{\Omega}Jv''-J\ddot{w}''=0 \tag{2.6}$$

Boundary conditions are as follows

At x=0

$$v=w=0,\quad v'=w'=0 \tag{2.7a}$$

At x=L

$$EIv'''+Mv\Omega^2+2Jv'\Omega^2+2Mw\dot{\Omega}-M\ddot{v}+Mw\dot{\Omega}-\dot{\Omega}Jw'-J\ddot{v}'=-\frac{\varepsilon A_v V_{DC}^2}{2(d_v-v)^2} \tag{2.7b}$$

$$EIw'''+Mw\Omega^2+2Jw'\Omega^2-2Mv\dot{\Omega}-M\ddot{w}-Mv\dot{\Omega}-\dot{\Omega}Jv'-J\ddot{w}'=-\frac{\varepsilon A_w(V_{DC}+V_{\acute{A}C})^2}{2(d_w-w)^2} \tag{2.7c}$$

$$EIv''=0,\ EIw''=0 \tag{2.7d}$$

The general equation of motion are reduced to nondimensional form by using some constant, which are defined in this section. By using this constant the general equation of motion converted into nondimensional form. For simplification of the above equation the following terms are described

$$\hat{x} = \frac{x}{L}, \quad \hat{v} = \frac{v}{d_v}, \quad \hat{w} = \frac{w}{d_w}, \quad d = \frac{d_v}{d_w}, \quad \hat{t} = \tau t, \tag{2.8a}$$

$$\hat{\Omega} = \frac{\Omega}{\tau}, \quad \hat{J} = \frac{J}{mL^2}, \quad \alpha_v = \frac{\varepsilon A_v L^3}{2EId_v^3}, \quad \alpha_w = \frac{\varepsilon A_w L^3}{2EId_w^3}, \tag{2.8b}$$

$$M_r = \frac{M}{mL}, \quad \tau = \sqrt{\frac{EI}{mL^4}}, \tag{2.8c}$$

Then, the equation and boundary conditions convert into nondimensional form as follows:

$$v^{iv} + c\dot{v} - \Omega^2 v + 2J\Omega^2 v'' - 2\frac{\Omega}{d}\dot{w} + \ddot{v} - \frac{\dot{\Omega}}{d}w - \frac{J\dot{\Omega}}{d}w'' - J\ddot{v}'' = 0 \tag{2.9}$$

$$w^{iv} + c\dot{w} - \Omega^2 w + 2J\Omega^2 w'' + 2\Omega d\dot{v} + \ddot{w} + \dot{\Omega}dv - \dot{\Omega}dJv'' - J\ddot{w}'' = 0 \tag{2.10}$$

At x=0

$$v = w = 0 \quad \text{and} \quad v' = w' = 0 \tag{2.11a}$$

At x=1, $\quad v'' = w'' = 0$ (2.11b)

$$v''' + M_r\Omega^2 v + 2J\Omega^2 v' + 2\frac{M_r\Omega}{d}\dot{w} - M_r\ddot{v} + \frac{M_r\dot{\Omega}}{d}w - \frac{J\dot{\Omega}}{d}w' - J\ddot{v}' = -\alpha_v \frac{V_{DC}^2}{(1-v)^2} \tag{2.11c}$$

$$w''' + M_r\Omega^2 w + 2J\Omega^2 w' - 2M_r\Omega d\dot{v} - M_r\ddot{w} - M_r\dot{\Omega}dv - J\dot{\Omega}dv' - J\ddot{w}' = -\alpha_w \frac{(V_{DC} + V_{AC})^2}{(1-w)^2} \tag{2.11d}$$

2.3 Intermolecular forces

Casimir force and van der Waal forces considered as intermolecular forces. When the distance between the proof mass and electrode is in the order of 100nm to 1000nm, then Casmir forces as well as van der Waal forces have major impact on the system and these forces affect the performance of the gyroscope. When two plates are parallel and hold apart from each other, then Casmir force can be written as:

$$F_c = \frac{\pi^2 hc}{240 h_g^4} \tag{2.12}$$

Where, F_c= Casmir forces per unit area, c= speed of light, h= Planck's constant divided by 2π, h_g = distance between the plates. Using equation 7 we can rewrite the effect of Casmir force on the proof mass in drive and sense direction respectively as follows:

$$F_{1c} = \frac{\pi^2 A_w hc}{240(d_w - w)^4} \tag{2.13a}$$

$$F_{2c} = \frac{\pi^2 A_v hc}{240(d_v - v)^4} \tag{2.13b}$$

where, F_{1c} and F_{2c} are the Casmir forces in the drive and sense direction respectively, A_w and A_v are the area of drive and sense electrode, d_w and d_v are the gap between the proof mass and drive and sense electrode respectively.

In this working range (100nm to 1000nm), the van der Waal's forces also affect the system and the gyroscope performance. For parallel plate the expression for the Van der Waal force is as follows:

$$F_{vdW} = \frac{H}{6\pi h_g^3} \tag{2.14}$$

where, F_{vdw}= Vander Waal force per unit area, H= Hamaker coefficient ranging between 10^{-19} to 10^{-20} J. using equation 10 the expression of Vander Waal force for tip mass can be written as follows:

$$F_{1vdW} = \frac{HA_w}{6\pi(d_w - w)^3} \tag{2.15a}$$

$$F_{2vdW} = \frac{HA_v}{6\pi(d_v - v)^3} \tag{2.15b}$$

Where, F_{1vdW} and F_{2vdW} are the Vander Waal forces in the drive and sense direction respectively.

2.4 Damping formulation

The damping for the micro devices depends upon several non-linear effects. Viscous damping present in the system because of air in the gyroscope cavity. Viscous damping decreases as the pressure of air reaches to vacuum. Here the viscous damping effects incorporated by using slide film and squeeze film damping model in drive and sense dome direction.

The effective viscosity μ_{SL} for the gas can be written as follows for slide film damping:

$$\mu_{SL} = \frac{\mu}{1 + 2K_n + 0.2K_n^{0.788}e^{-K_n/10}} \tag{2.16}$$

Where μ is the gas viscosity and K_n is Knudsen number, Knudsen number is the function of initial drive gap, d_w, and gas mean free path λ

$$K_n = \frac{\lambda}{d_w} \tag{2.17}$$

Where, λ for air can be obtained from following relation.

$$P\lambda = 6.777 \times 10^{-3} \text{ [Pa m]} \tag{2.18}$$

Where P is the air pressure, the slide film damping coefficients can be expressed as follows:

$$C_{SL} = \mu_{SL}\frac{A_w}{d_w} \tag{2.19}$$

Similarly, the effective gas viscosity can be written in form of Knudsen number.

$$\mu_{SQ} = \frac{\mu}{1 + 9.638K_n^{1.159}} \tag{2.20}$$

Knudsen number expression for sense direction

$$K_n = \frac{\lambda}{d_v} \tag{2.21}$$

The squeeze film damping coefficients can be written as follows:

$$C_{SQ} = 0.42\mu_{SQ}\frac{A_v^2}{d_v^3} \tag{2.22}$$

2.5 Static Analysis modelling

Static pull-in analysis is the first stage to the design of nano gyroscope. Static analysis help to fix the working region for the nano device. It provide the information about the maximum force can be apply to the system. For static analysis the nondimensional equations (2.9) and (2.10) are used. Here angular acceleration and time dependent terms are neglected and the equations are converted into static part. The detailed modelling of the static analysis equations are described below.

2.5.1 Modelling without Intermolecular Force

In order to obtain static solution, either equation (2.9) or (2.10) may be considered because it is assumed that $v_s = w_s$. Initially the static analysis equations are written without considering the effect of intermolecular forces for drive and sense direction individually are as follows:-

Let the static deflections along sense direction be $v_s(x)$ respectively. By eliminating the time derivatives in equation (2.9), the static uncoupled equilibrium equations is obtained in dimensionless form for the sense direction as:

$$v_s^{iv} - \Omega^2 v_s + 2J\Omega^2 v_s'' = 0 \tag{2.23}$$

Subject to boundary condition,

At x=0,

$$v_s(0) = 0 \tag{2.24a}$$

$$v_s'(0) = 0 \tag{2.24b}$$

At x=1,

$$v_s''(1) = 0 \tag{2.24c}$$

$$v_s'''(1) + M_r\Omega^2 v_s(1) + 2J\Omega^2 v_s'(1) = -\frac{\alpha_v V_{DC}^2}{(1-v_s(1))^2} \tag{2.24d}$$

The general solution can be expressed as

$$v_s(x) = c_1 e^{a_1 x} + c_2 e^{-a_1 x} + c_3 e^{a_2 x} + c_4 e^{-a_2 x} \tag{2.25}$$

Where,

$$a_{1,2} = \sqrt{-J\Omega^2 \pm \sqrt{J^2\Omega^4 + \Omega^2}} \tag{2.26}$$

2.5.2 Modelling with Intermolecular Force

The static analysis by considering the intermolecular forces along with the electrostatic force is similar to the static analysis without intermolecular forces, but the only difference in the boundary condition. For this analysis the intermolecular forces such as Casmir and wander Waals forces also considered in the equation of motion and boundary condition. The boundary condition which changes during this analysis are as follows and remaining boundary condition are remain same.

For sense direction

$$v_s'''(1) + M_r\Omega^2 v_s(1) + 2J\Omega^2 v_s'(1) = -\frac{\alpha_v V_{DC}^2}{(1-v_s(1))^2} - \kappa_1(F_{2c} + F_{2vdw}) \tag{2.27}$$

Where, κ_1, κ_2 are constant can define such as follows

$$\kappa_1 = \frac{L^3}{EId_v} \tag{2.28}$$

2.6 Natural frequency Analysis

The natural frequency for the system is calculated from the eigen value problem. The dynamic equation in drive direction can be written in terms of w_d where $\hat{w}(\hat{x},\hat{t}) = w_s(\hat{x}) + w_d(\hat{x},\hat{t})$ as follows

$$w_d^{iv} + \ddot{w}_d - \hat{J}\ddot{w}_d'' = 0 \tag{2.29}$$

And boundary conditions are as follows

at x=0,

$$w_d = 0, \quad w_d' = 0 \tag{2.30a}$$

at x=1,

$$w_d''' - M_r\ddot{w}_d - \hat{J}\ddot{w}_d' = -\frac{\alpha_w V_{DC}^2}{(1-w_d)^2} \tag{2.30b}$$

$$w_d'' = 0 \tag{2.30c}$$

The solution of the equation is assumed as follows:

$$w_d(\hat{x},\hat{t}) = \Phi(\hat{x})e^{i\omega\hat{t}} \tag{2.31}$$

Then the eige value problem is obtained as

$$\Phi^{iv}(\hat{x}) - \omega^2\Phi(\hat{x}) + \omega^2\hat{J}\Phi''(\hat{x}) = 0 \tag{2.32}$$

$$\Phi(0) = 0, \quad \Phi'(0) = 0 \tag{2.33a}$$

$$\Phi''(1) = 0 \tag{2.33b}$$

$$\Phi'''(1) + \omega^2 M_r\Phi(1) + \omega^2 J\Phi'(1) = -\frac{2\alpha_v V_{Dc}^2\Phi(1)}{(1-w_s(1))^3} \tag{2.33c}$$

Where $w_s(1)$ is the static deflection at the end of the beam and the solution of the above equation can be written as follows

$$\Phi(\hat{x}) = A_1\sin\lambda_1 x + A_2\cos\lambda_1 x + A_3\sinh\lambda_2 x + A_4\cosh\lambda_2 x \tag{2.34}$$

Where

$$\lambda_1 = \sqrt{\frac{1}{2}(\omega\sqrt{\alpha^2\omega^2+4}+\alpha\omega^2)} \tag{2.35a}$$

$$\lambda_2 = \sqrt{\frac{1}{2}(\omega\sqrt{\alpha^2\omega^2+4}-\alpha\omega^2)} \tag{2.35b}$$

By substituting $\Phi(\hat{x})$ in boundary conditions equs. (2.33) and eliminating constants A_1 to A_4 by equating coefficients determinant to zero we get the frequency equation in terms of tip mass ratio M_r, DC voltage and ω. The pull-in voltage is obtained as a point where ω becomes zero.

2.7 Dynamic Analysis modelling

Dynamic analysis also have equal importance for the design and development of the nano gyroscope. Here we consider the damping effect and the time coordinate terms. Dynamic analysis provides the detailed information about response of the systems against the dynamic loading condition.

2.7.1 Lumped Parameter Modelling

The equivalent lumped model is shown in the fig. 2.3, Here the M_p is equivalent mass of the system and c_y, c_z, and K_y, K_z are the equivalent damping coefficients and stiffness in drive and sense direction.

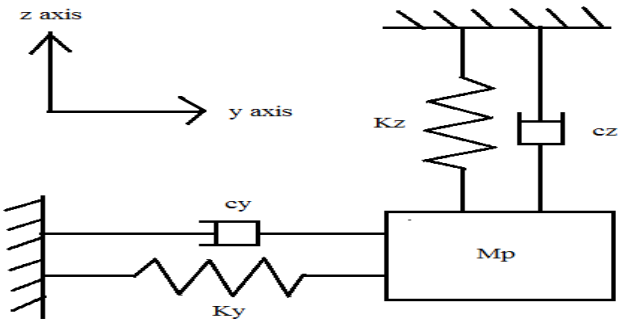

Fig. 2.3 Lumped parameter model

$$M_p\ddot{v} + c_y\dot{v} + (K_y - M_p\Omega^2)v - 2M_p\Omega\dot{w} - M_p\dot{\Omega}w = -\frac{\varepsilon A_v V_{DC}^2}{2(d_v - v)^2} \tag{2.36}$$

$$M_p\ddot{w} + c_z\dot{w} + (K_z - M_p\Omega^2)w + 2M_p\Omega\dot{v} + M_p\dot{\Omega}v = -\frac{\varepsilon A_w (V_{DC} + V_{AC})^2}{2(d_w - w)^2} \tag{2.37}$$

These oridinary differential equation can be solved by a numerical method. For solving continuous system of equations with intermolecular forces and damping forces, we have to use approximate method like Galerkin method or numerical finite element method.

2.7.2 Galerkin's Decomposition Technique

For using this method, first the modal analysis of the beam having tip mass at its end are performed and the mode shape function expression derived. The 4th order partial differential equation are reduced to 2nd order ordinary differential equation by using the Galerkin's order reduction technique. For Galerkin's technique the mode shape function expression is utilized for order reduction.

For this method first the solution of the equation are assumed in the form of displacement and time domain. There are two bending direction for these case then the solution of the equation for both the bending direction are as follows:

$$v(x,t) = \sum_{r=1}^{N} q_1(t)\phi_r(x) \tag{2.38a}$$

$$w(x,t) = \sum_{r=1}^{N} q_2(t)\phi_r(x) \tag{2.38b}$$

Where the N shows the no. of mode consider for the analysis and $\phi_r(x)$ is the mode shape function. The beam is fixed at one end and a small proof mass is attached to its other end. The

mode shape function is derived by considering the Euler-Bernoulli beam theory. The mode shape function is used to convert the partial differential equation into ordinary differential equation. The higher order differential equation is converted into lower order by using mode shape function. The mode shape function for the cantilever beam having tip mass at its end for r^{th} vibration mode can be written as follows:

$$\phi_r(x) = A_r\left[\cos\frac{\lambda_r}{L}x - \cosh\frac{\lambda_r}{L}x + \varsigma_r\left(\sin\frac{\lambda_r}{L}x - \sinh\frac{\lambda_r}{L}x\right)\right] \tag{2.39}$$

Here,

$$\varsigma_r = \frac{\sin\lambda_r - \sinh\lambda_r + \lambda_r\frac{M}{mL}(\cos\lambda_r - \cosh\lambda_r)}{\cos\lambda_r + \cosh\lambda_r - \lambda_r\frac{M}{mL}(\sin\lambda_r - \sinh\lambda_r)} \tag{2.40}$$

λ_r Can be calculated from the equation

$$1 + \cos\lambda_r\cosh\lambda_r + \lambda_r\frac{M}{mL}(\cos\lambda_r\sinh\lambda_r - \sin\lambda_r\cosh\lambda_r) = 0 \tag{2.41}$$

Here two bending direction but due to symmetric beam the mode shape function for each bending direction is same and analysis is performed by considering only single mode.

$\phi_r(x)$ is chosen such that,

$$\int_0^L \phi_r^2(x)dx = 1 \tag{2.42}$$

The equation of motion are as follows:

$$EIv^{iv} + c\dot{x} - mv\Omega^2 + 2Jv''\Omega^2 - 2m\dot{w}\Omega + m\ddot{v} - mw\dot{\Omega} - \dot{\Omega}Jw'' - J\ddot{v}'' = -\frac{\varepsilon A_v V_{DC}^2}{2(d_v - v)^2} \tag{2.43}$$

$$EIw^{iv} + c\dot{w} - mw\Omega^2 + 2Jw''\Omega + 2m\dot{v}\Omega + m\ddot{w} + mv\dot{\Omega} - \dot{\Omega}Jv'' - J\ddot{w}'' = -\frac{\varepsilon A_w (V_{DC} + V_{AC})^2}{2(d_w - w)^2} \quad (2.44)$$

By neglecting some terms then the equations are reduced as follows:

$$EIv^{iv} + c\dot{v} - mv\Omega^2 + 2Jv''\Omega^2 - 2m\dot{w}\Omega + m\ddot{v} - J\ddot{v}'' = -\frac{\varepsilon A_v V_{DC}^2}{2(d_v - v)^2} \quad (2.45)$$

$$EIw^{iv} + c\dot{w} - mw\Omega^2 + 2Jw''\Omega + 2m\dot{v}\Omega + m\ddot{w} - J\ddot{w}'' = -\frac{\varepsilon A_w (V_{DC} + V_{AC})^2}{2(d_w - w)^2} \quad (2.46)$$

The solution of the equation can be rewrite as follows:

$$v(x,t) = q_1(t)\phi(x) \quad (2.47a)$$

$$w(x,t) = q_2(t)\phi(x) \quad (2.47b)$$

Derivatives are as follows:

$v(x,t) = q_1(t)\phi(x)$, $w(x,t) = q_2(t)\phi(x)$

$v^{iv}(x,t) = q_1(t)\phi^{iv}(x)$, $w^{iv}(x,t) = q_2(t)\phi^{iv}(x)$

$\dot{v}(x,t) = \dot{q}_1(t)\phi(x)$, $\dot{w}(x,t) = \dot{q}_2(t)\phi(x)$

$v''(x,t) = q_1(t)\phi''(x)$, $w''(x,t) = q_2(t)\phi''(x)$

$\ddot{v}(x,t) = \ddot{q}_1(t)\phi(x)$, $\ddot{w}(x,t) = \ddot{q}_2(t)\phi(x)$

$$\ddot{v}''(x,t) = \ddot{q}_1(t)\phi''(x), \quad \ddot{w}''(x,t) = \ddot{q}_2(t)\phi''(x) \quad (2.48)$$

2.7.3 Reduced order equation

The order of the equation are reduced by using Galerkin's decomposition technique, which is described in above section.by using the proper substitution of parameters and adopting step by step procedure the order of the equation of motion are reduced as follows The above derivatives are substitute in the equation 2.36 and 2.37

$$EI[q_1(t)\phi^{iv}(x)]+c[\dot{q}_1(t)\phi(x)]-m\Omega^2[q_1(t)\phi(x)]+2J\Omega^2[q_1(t)\phi''(x)]-2m\Omega[\dot{q}_2(t)\phi(x)]$$
$$+m[\ddot{q}_1(t)\phi(x)]-J[\ddot{q}_1(t)\phi''(x)]=-\frac{\varepsilon A_v V_{DC}^2}{2d_v^2}[1+\frac{2q_1(t)\phi(x)}{d_v}]$$

Here $\phi^{iv}(x)=\left(\frac{\lambda}{L}\right)^4\phi(x)$ so the equation reduced to

$$EI[q_1(t)\left(\frac{\lambda}{L}\right)^4\phi(x)]+c[\dot{q}_1(t)\phi(x)]-m\Omega^2[q_1(t)\phi(x)]+2J\Omega^2[q_1(t)\phi''(x)]-2m\Omega[\dot{q}_2(t)\phi(x)]$$
$$+m[\ddot{q}_1(t)\phi(x)]-J[\ddot{q}_1(t)\phi''(x)]=-\frac{\varepsilon A_v V_{DC}^2}{2d_v^2}[1+\frac{2q_1(t)\phi(x)}{d_v}]$$

Integrating both side with respect to x and $\phi(x)$ is multiplied both the side

$$EI\left(\frac{\lambda}{L}\right)^4 q_1(t)\left[\int_0^L\phi^2(x)dx\right]+c\dot{q}_1(t)\left[\int_0^L\phi^2(x)dx\right]-m\Omega^2q_1(t)\left[\int_0^L\phi^2(x)dx\right]$$
$$+2J\Omega^2q_1(t)\left[\int_0^L\phi(x)\phi''(x)dx\right]-2m\Omega\dot{q}_2(t)\left[\int_0^L\phi^2(x)dx\right]+m\ddot{q}_1(t)\left[\int_0^L\phi^2(x)dx\right]$$
$$-J\ddot{q}_1(t)\left[\int_0^L\phi(x)\phi''(x)dx\right]=-\frac{\varepsilon A_v V_{DC}^2}{2d_v^2}\left(\left[\int_0^L\phi(x)dx\right]+\frac{2q_1(t)}{d_v}\left[\int_0^L\phi^2(x)dx\right]\right)$$

Since $\int_0^L\phi^2(x)dx=1$ and let take $a_{00}=\int_0^L\phi(x)\phi''(x)dx$ and $a_{01}=\int_0^L\phi(x)dx$

$$EI\left(\frac{\lambda}{L}\right)^4 q_1(t)+c\dot{q}_1(t)-m\Omega^2 q_1(t)+2J\Omega^2 q_1(t)a_{00}$$

$$-2m\Omega\dot{q}_2(t)+m\ddot{q}_1(t)-J\ddot{q}_1(t)a_{00}=-\frac{\varepsilon A_v V_{DC}^2}{2d_v^2}\left(a_{01}+\frac{2q_1(t)}{d_v}\right)$$

Or can be rewrite as:

$$\begin{aligned}&\left[m-J\left(a_{00}\right)\right]\ddot{q}_1(t)+\left[c\right]\dot{q}_1(t)+\left[EI\left(\frac{\lambda}{L}\right)^4+2J\Omega^2\left(a_{00}\right)-m\Omega^2+\frac{\varepsilon A_v V_{DC}^2}{d_v^3}\right]q_1(t)\\&-\left[2m\Omega\right]\dot{q}_2(t)=-\frac{\varepsilon A_v V_{DC}^2}{2d_v^2}\left[a_{01}\right]\end{aligned}\tag{2.49}$$

Similarly in drive direction the equation reduced as follows:

$$\begin{aligned}&\left[m-J\left(a_{00}\right)\right]\ddot{q}_2(t)+\left[c\right]\dot{q}_2(t)+\left[EI\left(\frac{\lambda}{L}\right)^4+2J\Omega^2\left(a_{00}\right)-m\Omega^2+\frac{\varepsilon A_w\left(V_{DC}+V_{AC}\right)^2}{d_w^3}\right]q_2(t)\\&+\left[2m\Omega\right]\dot{q}_1(t)=-\frac{\varepsilon A_w\left(V_{DC}+V_{AC}\right)^2}{2d_w^2}\left[a_{01}\right]\end{aligned}\tag{2.50}$$

2.7.4 Finite Element Method

Here a cantilever beam having tip mass is considered and it's loaded in two perpendicular direction by electrostatic forces which is shown in Fig.2.4

Let beam length is L, width b and thickness h, beam has rectangular cross-section so area A=b. h, the beam is made by isotropic and linear elastic material having density ρ, young's modulus E poisons ratio υ, mass m_b=L.h.b. ρ and shear modulus G = $\frac{E}{2(\nu+1)}$

For finite element modelling we consider N element each element having length l = $\frac{L}{N}$ and mass

$$m_e=\frac{m_b}{N}$$

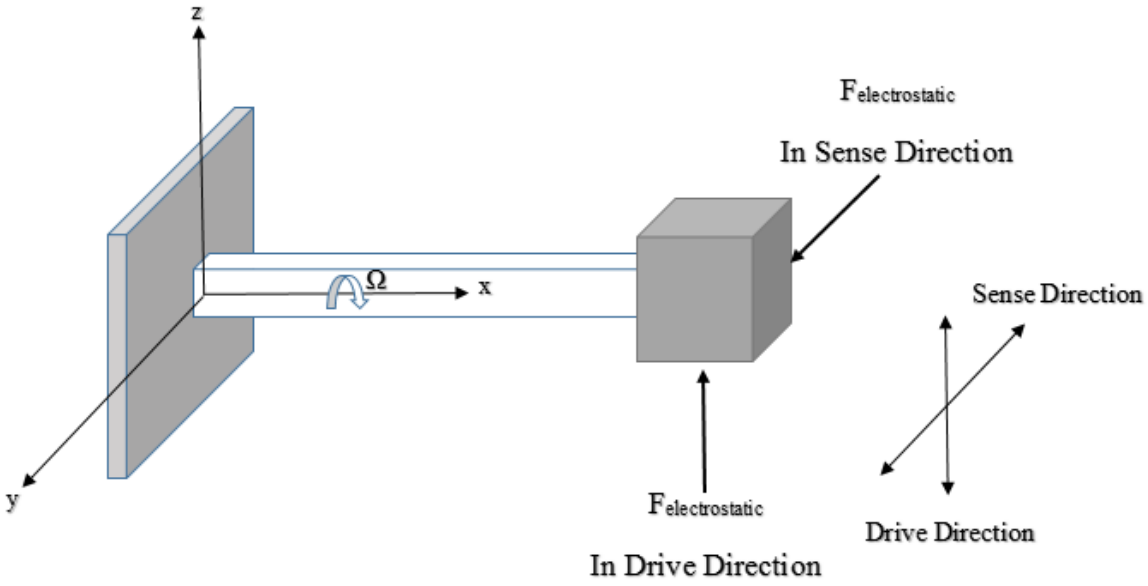

Fig. 2.4 Cantilever beam with loading conditions

For 3-D case each node having 6 degree of freedom such as 3 translational displacement u, v and w along x, y and z axis respectively and 6 rotational degree of freedom α, β and γ with respect to x, y and z axis.

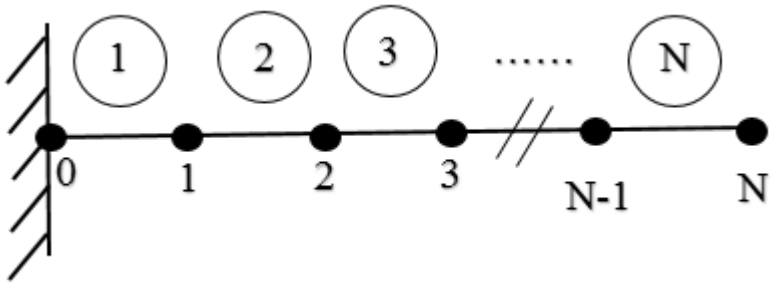

Fig. 2.5 Global numbering of the element

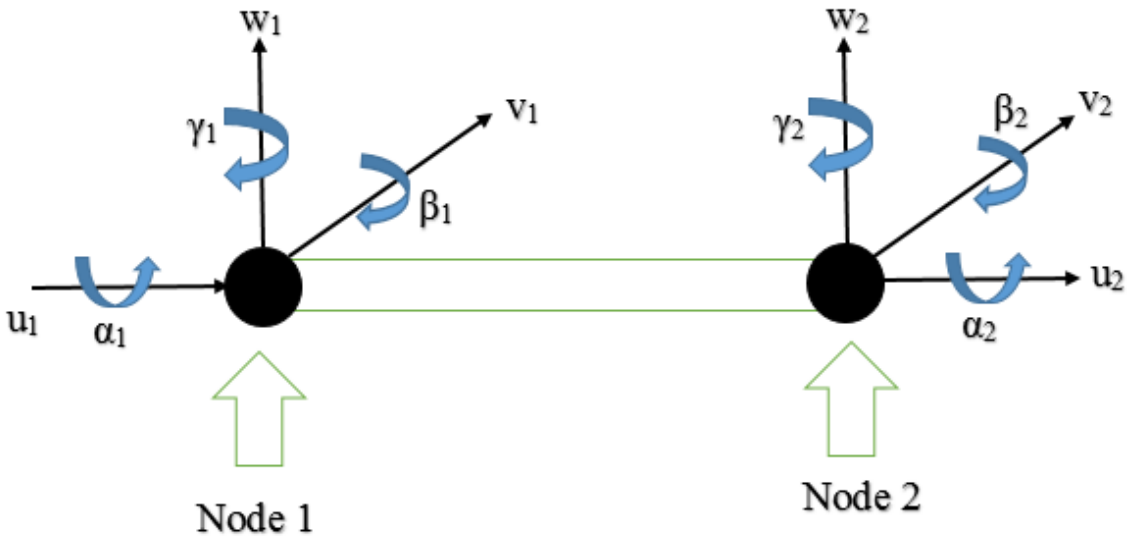

Fig. 2.6 Local degree of freedom for beam element

The second moment of inertia for the element about y and z and polar moment of inertia about x axis are as follows:

$$I_y = \frac{bh^3}{12} \quad I_z = \frac{b^3 h}{12} \quad I_p = \frac{(b^2 + h^2)}{12} \frac{m}{N} \tag{2.51}$$

The exact analytical value for the element torsion constant I_t in not exist so the approximate value is taken from the literature survey are as follows:

$$I_t = 0.141 bh^3, \quad \text{if} \quad h < b \quad \text{or} \quad I_t = 0.141 b^3 h \quad \text{if} \quad h > b \tag{2.52}$$

For simplification

$$p_y = \frac{12EI_z}{GA_{s,y}l^2} \qquad p_z = \frac{12EI_y}{GA_{s,z}l^2} \tag{2.53}$$

Where $A_{s,y} = A_{s,z} = \frac{5}{6} t.h$ are the effective shear area for rectangular cross-section.

The local mass and stiffness are M_{11}^e and K_{11}^e for the Timoshenko beam element which is considered for modelling. We have consider 12 local degree of freedom for element and 6 dofs for each node. So the elemental mass and stiffness matrix are as follows.

$$M^e = \begin{bmatrix} M_{11}^e & M_{12}^e \\ M_{21}^e & M_{22}^e \end{bmatrix}, \; K^e = \begin{bmatrix} K_{11}^e & K_{12}^e \\ K_{21}^e & K_{22}^e \end{bmatrix} \tag{2.54}$$

Where $(\cdot)_{11}^e$ and $(\cdot)_{22}^e$ represents the interdependency of the dofs between first and second node and $(\cdot)_{12}^e = (\cdot)_{21}^e$ shows the interconnection between the nodes. M_{22}^e and K_{22}^e are equal to M_{11}^e and K_{11}^e respectively except the sign of the off

$$M_{11}^e = m_e \begin{bmatrix} \frac{1}{3} & 0 & 0 & 0 & 0 & 0 \\ 0 & \frac{13}{35} + \frac{6I_z}{5Al^2} & 0 & 0 & 0 & \frac{11l}{210} + \frac{I_z}{10Al} \\ 0 & 0 & \frac{13}{35} + \frac{6I_y}{5Al^2} & 0 & -\frac{11l}{210} - \frac{I_y}{10Al} & 0 \\ 0 & 0 & 0 & \frac{I_p}{3A} & 0 & 0 \\ 0 & 0 & -\frac{11l}{210} - \frac{I_y}{10Al} & 0 & \frac{l^2}{105} + \frac{2I_y}{15A} & 0 \\ 0 & \frac{11l}{210} + \frac{I_z}{10Al} & 0 & 0 & 0 & \frac{l^2}{105} + \frac{2I_z}{15A} \end{bmatrix} \tag{2.55}$$

$$M_{21}^{e} = M_{12}^{e\,T} = m_e \begin{bmatrix} \frac{1}{6} & 0 & 0 & 0 & 0 & 0 \\ 0 & \frac{9}{70} - \frac{6I_z}{5Al^2} & 0 & 0 & 0 & \frac{13l}{420} - \frac{I_z}{10Al} \\ 0 & 0 & \frac{9}{70} - \frac{6I_y}{5Al^2} & 0 & -\frac{13l}{420} + \frac{I_y}{10Al} & 0 \\ 0 & 0 & 0 & \frac{I_p}{6A} & 0 & 0 \\ 0 & 0 & \frac{13l}{420} - \frac{I_y}{10Al} & 0 & -\frac{l^2}{140} - \frac{2I_y}{30A} & 0 \\ 0 & -\frac{13l}{420} + \frac{I_z}{10Al} & 0 & 0 & 0 & -\frac{l^2}{140} - \frac{2I_z}{30A} \end{bmatrix} \tag{2.56}$$

$$K_{11}^{e} = \frac{1}{l^3} \begin{bmatrix} EAl^2 & 0 & 0 & 0 & 0 & 0 \\ 0 & \frac{12EI_z}{1+P_y} & 0 & 0 & 0 & \frac{6EI_z l}{1+P_y} \\ 0 & 0 & \frac{12EI_y}{1+P_z} & 0 & -\frac{6EI_y l}{1+P_z} & 0 \\ 0 & 0 & 0 & GI_t l^2 & 0 & 0 \\ 0 & 0 & -\frac{6EI_y l}{1+P_z} & 0 & \frac{EI_y l^2 (4+P_z)}{1+P_z} & 0 \\ 0 & \frac{6EI_z l}{1+P_y} & 0 & 0 & 0 & \frac{EI_z l^2 (4+P_y)}{1+P_y} \end{bmatrix} \tag{2.57}$$

$$K_{21}^{e} = K_{12}^{e\,T} = \frac{1}{l^3}\begin{bmatrix} -EAl^2 & 0 & 0 & 0 & 0 & 0 \\ 0 & -\frac{12EI_z}{1+P_y} & 0 & 0 & 0 & -\frac{6EI_z l}{1+P_y} \\ 0 & 0 & -\frac{12EI_y}{1+P_z} & 0 & \frac{6EI_y l}{1+P_z} & 0 \\ 0 & 0 & 0 & -GI_t l^2 & 0 & 0 \\ 0 & 0 & -\frac{6EI_y l}{1+P_z} & 0 & \frac{EI_y l^2(2-P_z)}{1+P_z} & 0 \\ 0 & \frac{6EI_z l}{1+P_y} & 0 & 0 & 0 & \frac{EI_z l^2(2-P_y)}{1+P_y} \end{bmatrix} \quad (2.58)$$

Above matrices are assembled to form global mass and stiffness of the beam with appropriate boundary conditions including tip mass. At the tip node, the displacement varying electrostatic and intermolecular forces are applied. The resultant equations are expressed as

$$M\ddot{X} + C\dot{X} + KX = F \quad (59)$$

Where C is the damping matrix and F is the force vector.

-----o-----

CHAPTER 3

RESULTS AND DISCUSSION

3.1 Static pull-in analysis

Pull-in is the very important phenomenon for design and analysis of micro/nano gyroscope. Here beam is used, so beam is deforming continuously due to applied voltage and base rotation. In the deformation process two forces are acting simultaneously such as deforming forces and restoring forces. When deforming forces exceeds to the maximum limit then the complete deformation take place and the beam will not regain its original position and the complete system will not work, so the pull-in analysis gives a limiting value beyond that limit system will fail. So pull-in analysis play very important role to finalize the working region. Generally pull-in will occurs at one third of initial gap.

3.1.1 Analysis without Intermolecular Forces

First the static pull-in analysis performed without considering the effect of intermolecular forces. Table 3.1 represent the data considered for static pull-in analysis. The complete formulation for the pull-in analysis is discussed in previous chapter mathematical modelling.

Table 3.1 Numerical data used for static pull-in Analysis

S. No	Parameter	Numerical value
1.	Beam length in m, L	400×10^{-6}
2.	Density of the beam and tip mass material in kg/m^3, ρ	2300
3.	Young's modulus in N/m^2, E	160×10^{9}
4.	Mass per unit length of the beam in kg/m, m	1.803×10^{-8}
5.	Tip mass in kg, M	7.2128×10^{-12}

6.	Width of the beam in m, b	2.8×10^{-6}
7.	Thickness of the beam in m, h	2.8×10^{-6}
8.	Initial gap between tip mass and sense electrode in m, d_v	2×10^{-6}
9.	Initial gap between tip mass and drive electrode in m, d_w	2×10^{-6}
10.	Area of the sense electrode in m^2, A_v	392×10^{-12}
11.	Area of the drive electrode in m^2, A_w	392×10^{-12}
12.	Vacuum electrical permittivity, ε	8.8542×10^{-12}
13.	Initial base rotation velocity in rad/sec, Ω	20

MATLAB toolbox is used to solve the equation and find the voltage verses displacement response. Initially the pull-in curve drawn without considering the intermolecular forces. Following code is used for MATLAB simulation.

```
%%%%%%%%plot Vdc verses nondimensional displacement%%%%%%%%
Rho=2330; % density of the beam and tip mass material in kg/m^3
O=20; %input rotation of the beam along x axis in rad/sec
b=2.8e-6; %width of the beam in m
Ar=392e-12; %area of electrode in m^2
L=400e-6; %length of beam in m
E=160e9; % elastic modulus of the beam material in N/m^2
Ee=8.8542e-12; %electrical permittivity
dv=2e-6; % gap between tip mass and drive electrode in m
M=7.2128e-12; % tip mass in kg
m=1.803e-8; % beam mass per unit length in kg/m
c=Rho*(b^2)*(1/6);
d=m*(L^2);
J=c/d; %polar moment of inertia
Mr=M/(m*L); %tip mass to beam mass ratio
I=(b^4)/12; %moment of inertia
t=sqrt((E*I)/(m*(L^4)));
Omega=(O/t);
d1=(-J*(Omega)^2);d2=sqrt(((J^2)*(Omega)^4)+(Omega^2));
AV=(Ee*Ar*L^3)/(2*E*I*(dv^3));
a1=sqrt(d1+d2);a2=sqrt(d1-d2);
i=1;
for Vm=0:0.05:1
A=[1,1,1,1;a1,-a1,a2,-a2;(a1^2*exp(a1)),(a1^2*exp(-
a1)),(a2^2*exp(a2)),(a2^2*exp(-a2));exp(a1),exp(-a1),exp(a2),exp(-a2)];
vm=[0;0;0;Vm];
C=inv(A)*vm;c1=C(1);c2=C(2);c3=C(3);c4=C(4);
```

```
p=(((a1^3)*(exp(a1))*c1)-((a1^3)*(exp(-a1))*c2)+((a2^3)*(exp(a2))*c3)-
((a2^3)*(exp(-a2))*c4));
q=(2*J*(Omega^2))*(((a1)*exp(a1)*c1)-((a1)*exp(-a1)*c2)+((a2)*exp(a2)*c3)-
((a2)*exp(-a2)*c4));
Vdc(i)=real(sqrt((((1-Vm)^2))*(1/(-AV))*(p+((Mr)*(Omega^2)*Vm)+q)));
i=i+1;
end
Vm1=0:0.05:1;
   plot(Vdc,Vm1,'-*r','linewidth',2);
   xlabel('DC Voltage Vdc');
   ylabel('Displacement Vm or Wm');
   %%%%%%%%%%%%%%%%%%%%%%%%%%%%%%%%%%%%%%%%%%%%%%%%%%%%%%%%%%%%%%%%%%%%%%
```

Fig. 3.1 shows the pull-in curve for the vibratory beam gyroscope without considering the effect of intermolecular forces and the AC voltage Vac=0 V. Pull-in curve is nothing but the response of nondimensional deflection verses applied DC voltage.

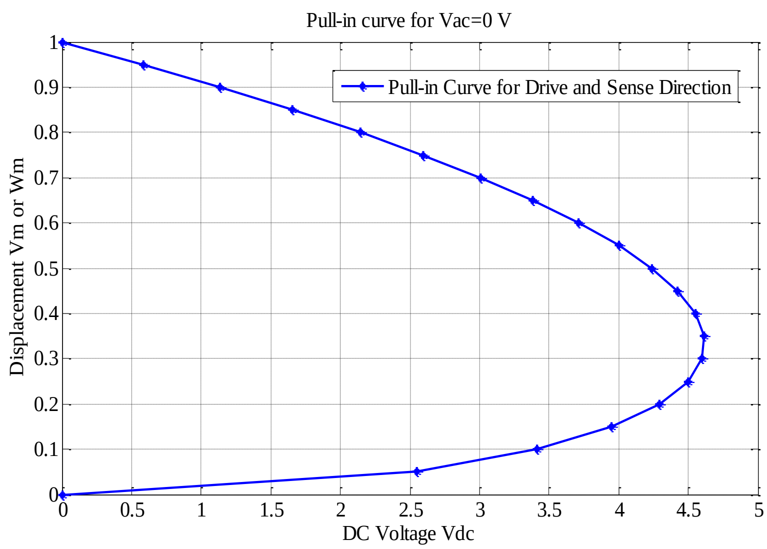

Fig. 3.1 Response of DC voltage v/s nondimensional deflection in drive and sense direction

3.1.2 Analysis with intermolecular forces

Static pull-in analysis with considering the effect of intermolecular forces is similar to the static pull-in analysis without considering the effect of intermolecular forces, but the only difference in the mathematical formulation of the system. Here the intermolecular forces such as Casimir force and Van der Waal's forces also consider along with the electrostatic forces. The detail formulation

has been discussed in mathematical modelling chapter. Table 3.2 shows the data used for numerical simulation task by considering the intermolecular forces.

Table 3.2 Numerical data used for Analysis with intermolecular forces

S. No.	Parameter	Numerical value
1.	Planck's constant in m^2kg/sec, h	1.0408×10^{-33}
2.	Speed of light in m/sec, c	3×10^{8}
3.	Hamaker coefficient in J, H	10^{-19}

MATLAB symbolic logic toolbox is used for the simulation task by considering the effect of intermolecular forces. Similar pseudo codes, which is discussed in previous section is used for analysis. Here the combined effect of intermolecular forces and electrostatic forces considered.

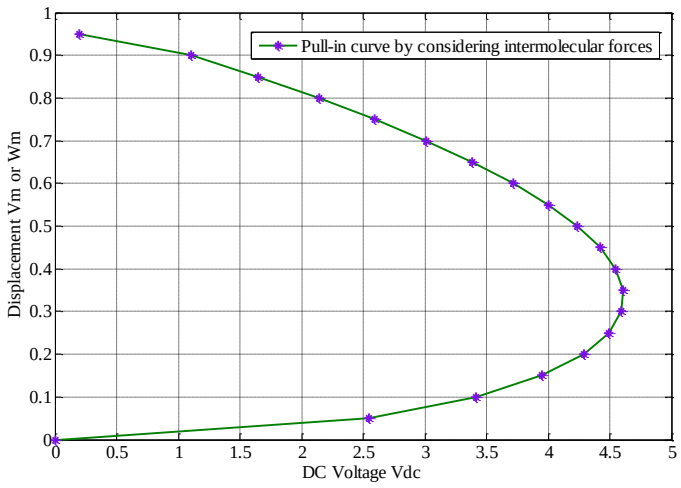

Fig. 3.2 Pull-in curve with intermolecular forces

Fig. 3.2 represent the response of the applied voltage verses nondimensional voltage by considering the effect of the intermolecular forces. Fig. 3.3 shows the comparison between the pull-in curve drawn by considering the effect of intermolecular forces and without considering the

intermolecular forces and fig. 3.4 represent the enlarged view of the fig. 3.3 which is clearly shows the difference of the pull-in curve by considering with and without intermolecular forces.

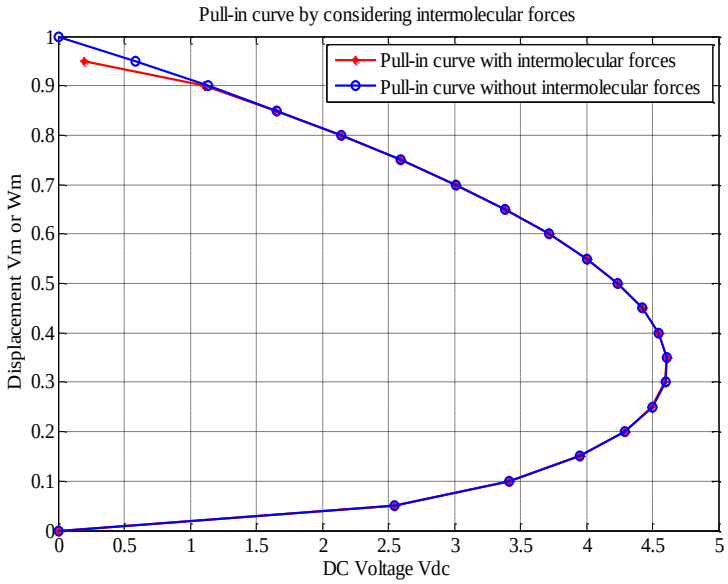

Fig. 3.3 Comparison Response of the DC voltage v/s nondimensional deflection with and without considering the effect of the intermolecular forces

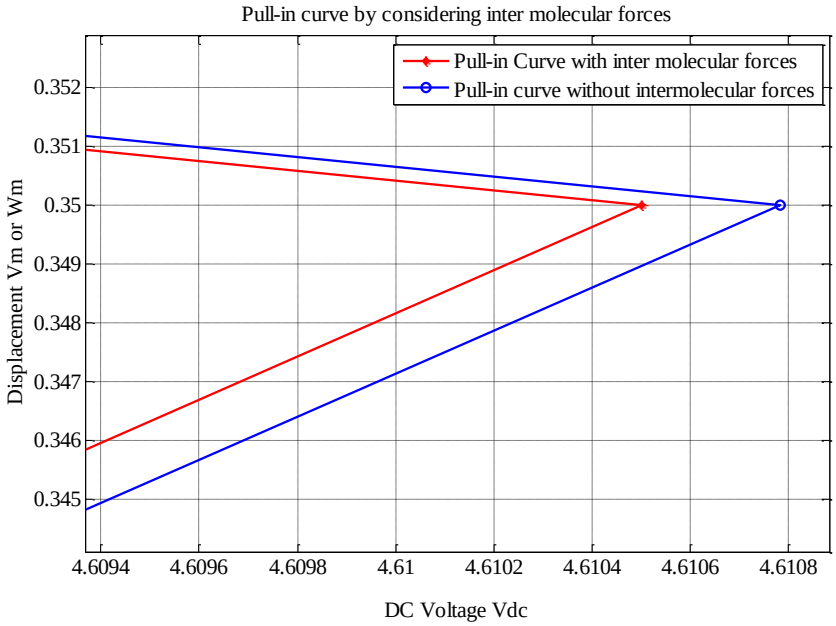

Fig. 3.4 Comparison b/w pull-in curve with and without considering the intermolecular forces

3.1.3 Effect of different parameter on pull-in curve

In previous sections the pull-in curve are drawn for different loading conditions and comparison made between them. In this section the effect of different parameter on the pull-in curve observed and investigate the corresponding change in pull-in voltage. Here the response of applied DC voltage verses nondimensional deflection also recorded due to change in different parameter.

3.1.3a Input Angular frequency

The beam is having two bending direction and the beam is spinning about the longitudinal axis. This spinning speed is known as the input angular frequency which is having major impact on the performance of the vibratory beam type gyroscope. The similar pseudo code is used for simulation which is discussed in previous section. Here the different value of input angular frequency such as 15 rad/sec, 20 rad/sec and 25 rad/sec are taken for the comparison.

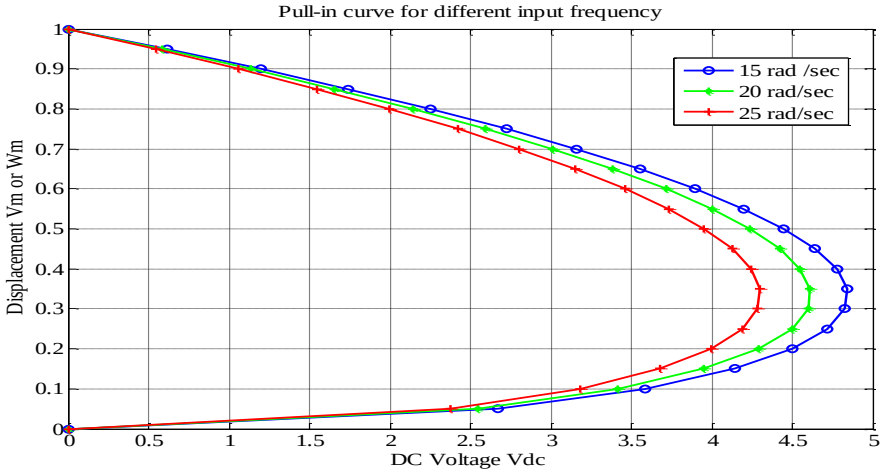

Fig. 3.5 Pull-in curve for different value of input angular frequencies

Fig.3.5 shows the variation of pull-in curve for different value of input angular frequencies, so here one important investigation made that the pull-in voltage value decreased by increase in input angular frequency.

3.1.3b Length of beam

In this work the tip mass is having extreme importance and the cantilever beam is used to support the tip mass. The length of this beam also affect the pull-in behaviour of the gyroscope. Here the length of beam taken as 380, 400 and 420 micron for comparison. Fig. 3.6 represents the pull-in behaviour of the gyroscope under different value of the beam length and it is observed that with increase the length of the beam the pull-in voltage decreased.

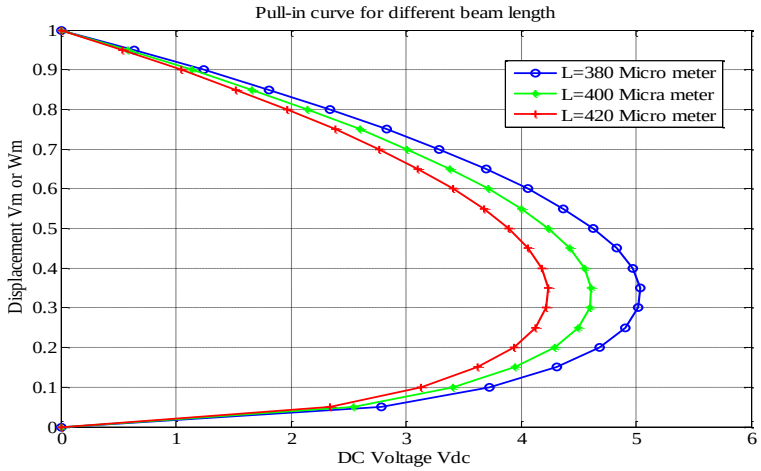

Fig. 3.6 Pull-in curve for different value of beam length

3.1.3c Width of beam

Width of the beam also affect the pull-in behaviour of the gyroscope. The different value of beam width 2.6, 2.8 and 3 micron for comparison. Fig. 3.7 shows the variation of pull-in curve for different value of width of the beam, here that can be observed that the pull-in voltage value increases due to increase in width of the beam.

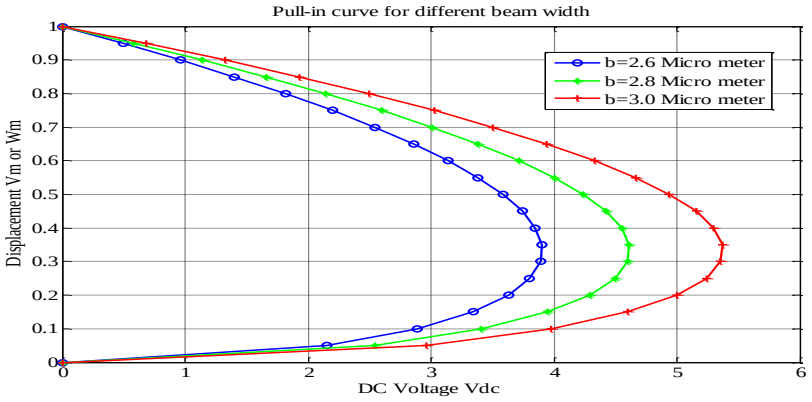

Fig. 3.7 Pull-in curve for different value of the width of the beam

3.1.3d Electrode Area

The area of the drive and sense electrode also having major impact on the pull-in curve. The different value of the area of electrode such as 372,392 and 412 micro m^2 are taken for the comparison. Fig. 3.8 shows the variation of pull-in curve due to different value of the drive and sense electrode. From the fig. 3.8 it is concluded that the pull-in voltage decreases with increase in electrode area.

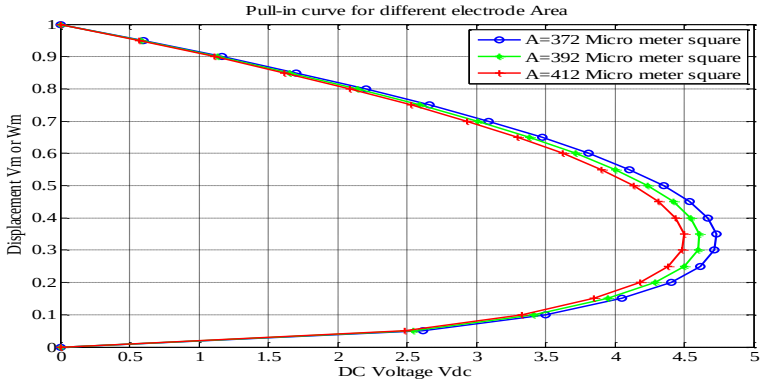

Fig. 3.8 Variation of pull-in curve with different value of electrode area

3.1.3e Gap between tip mass and electrode

Gap between the tip mass and the electrode also affect the pull-in curve. The different value of the gap between the electrode taken as 1.8, 2 and 2.2 micron. Fig, 3.9 shows the variation of pull-in

curve for the different gap between the electrode and tip mass. It is observed that the pull-in voltage increases by increase in the gap between the electrode and tip mass.

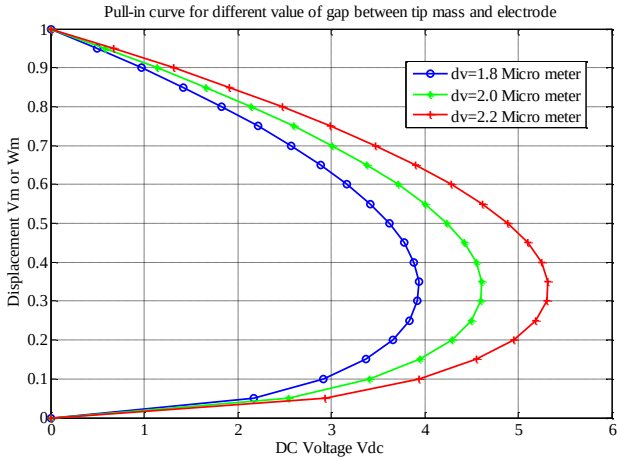

Fig. 3.9 Variation of pull-in curve with different value of gap b/w tip mass and electrode

3.1.3f Density change

Density of the material also affect the pull-in curve of the beam type gyroscope. The different value of the density such as 2300 kg/m^3 and 2330 kg/m^3 taken for the comparison. Fig. 3.10 shows with increase in density value the pull-in voltage value increases.

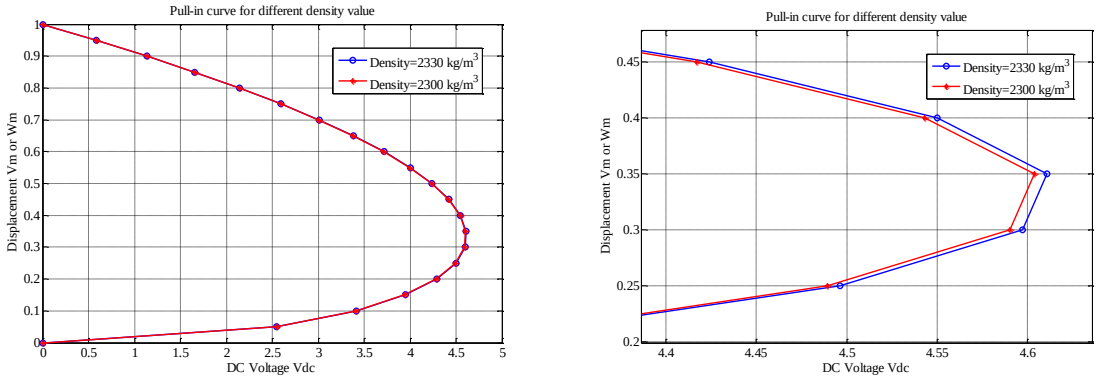

Fig. 3.10 Pull-in curve for different value of material density

Here we can made different conclusion from the above graphs. Table 3.3 represents the effect of pull-in voltage for the change in different parameter. The data taken from the above graphs and

tabulated below. Data shows that the pull-in voltage increases with increase in width of the beam and gap b/w the tip mass and electrode, while it decreases with increase in other parameter.

Table 3.3 Pull-in voltage for change in different parameter

S. No.	**Parameter change**	**Values**	**Corresponding pull-in voltage**	**Effect on pull-in voltage**
1.	Input angular velocity	15 rad/sec 20 rad/sec 25 rad/sec	4.8435 V 4.6149 V 4.3023 V	Voltage decreases by increase in input angular frequency
2.	Beam Length	380 micron 400 micron 420 micron	5.0401 V 4.6149 V 4.2378 V	Voltage decreases by increase in beam length
3.	Width of the beam	2.6 micron 2.8 micron 3.0 micron	3.9046 V 4.6149 V 5.3764 V	Voltage increases by increase in the width of beam
4.	Area of the Electrodes	372 micro m^2 392 micro m^2 412 micro m^2	4.7373 V 4.6149 V 4.5015 V	Voltage decreases by increase in electrode area
5.	Gap between tip mass and electrodes	1.8 micron 2.0 micron 2.2 micron	3.9402 V 4.6149 V 5.3241 V	Voltage increases by increase in gap b/w tip mass and electrode
6.	Density of material	2300 kg/m^3 2330 kg/m^3	4.6149 V 4.6079 V	Voltage decreases due to increase in density

3.2 Natural Frequency Analysis

Fundamental natural frequency vary with the applied DC voltage. In this section response of natural frequency verses applied DC voltage recorded due to change in different design parameter. Following pseudo code is used to solve the eigen value problem for fundamental natural frequency.

```
%%%%%EIGEN VALUE PROBLEM%%%%%
a=(ep*Av*L^3)/(2*E*I*dv^3);
JJ=(b^4)*(1/6);
J=JJ/(m*L^2);
Mr=M/m*L;
la1=sqrt((1/2)*((om*sqrt((a^2)*(om^2)+4))+a*(om^2)));
la2=sqrt((1/2)*((om*sqrt((a^2)*(om^2)+4))-a*(om^2)));
a11=0;a12=1;a13=0;a14=1;a21=la1;a22=0;a23=la2;a24=0;a31=-
la1^2*sin(la1);
a32=-la1^2*cos(la1);a33=la2^2*sinh(la2);a34=la2^2*cosh(la2);
a41=(-la1^3*cos(la1))+(J*om^2*la1*cos(la1))+(Mr*om^2*sin(la1))-
((2*Vdc^2*a*sin(la1))/(w - 1)^3);
a42=(la1^3*sin(la1))-(J*om^2*la1*sin(la1))+(Mr*om^2*cos(la1))-
((2*Vdc^2*a*cos(la1))/(w - 1)^3);
a43=(la2^3*cosh(la2))+(J*om^2*la2*cosh(la2))+(Mr*om^2*sinh(la2))
-(2*Vdc^2*a*(sinh(la2))/(w - 1)^3);
a44=(la2^3*sinh(la2))+(J*om^2*la2*sinh(la2))+(Mr*om^2*cosh(la2))
-(2*Vdc^2*a*(cosh(la2))/(w - 1)^3);
A=[a11,a12,a13,a14;a21,a22,a23,a24;a31,a32,a33,a34;a41,a42,a43,a
44];
p=eval(det(A))
i=1;
for om=0.001:0.001:1.1
p=eval(det(A))
Vdc1=eval(solve(p,Vdc))
vdc(i)=abs(Vdc1(1));
i=i+1;
end
ome=0.001:0.001:1.1;
plot(vdc,ome)
%%%%%%%%%%%%%%%%%%%%%%%%%%%%%%%%%%%%%%%%%%%%%%%%%%%%%%%%%%%%%%%%%%%%%%%
%%%%
```

The response of fundamental natural frequency verses the applied DC voltage recorded for different design parameter. Fig. 3.11 represent variation of frequency verses DC voltage for different mass ratio such as 0.1, 0.5 and 1.

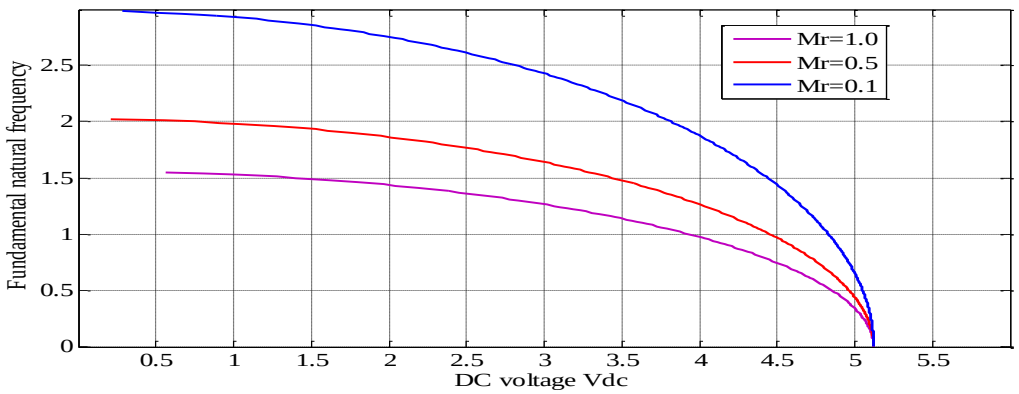

Fig. 3.11 Fundamental natural frequency v/s DC input voltage for different mass ratio

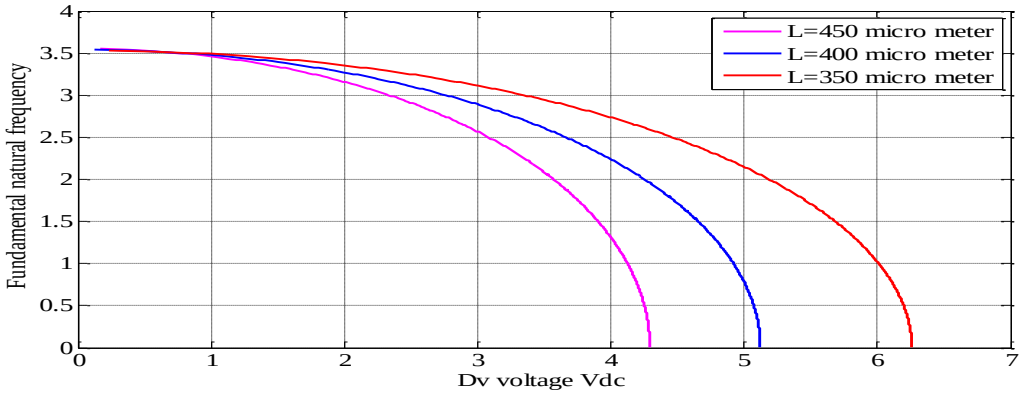

Fig. 3.12 Fundamental natural frequency v/s DC input voltage for different beam length

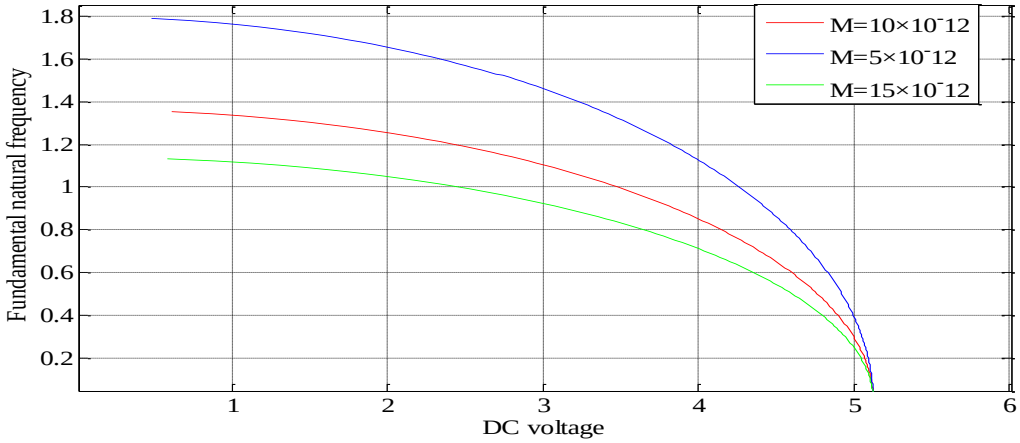

Fig. 3.13 Variation of the first natural frequency v/s DC voltage for different tip mass value

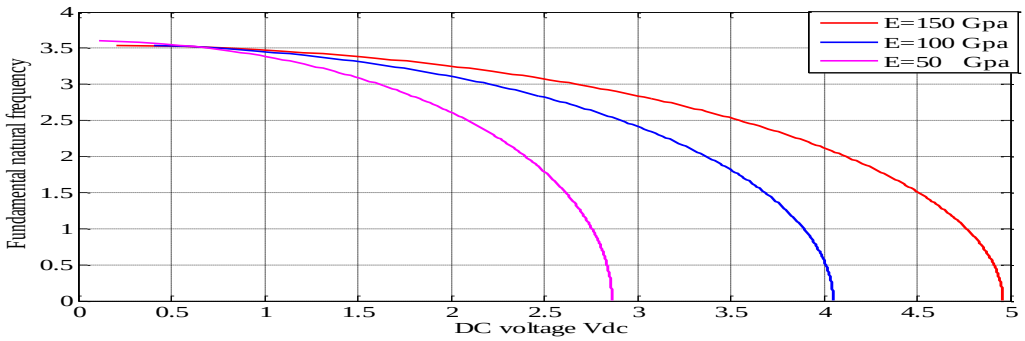

Fig. 3.14 Fundamental natural frequency v/s DC input voltage for different young's modulus

Fig. 3.12 represent the variation between frequency and DC voltage for different beam length such as 350, 400 and 450 micro meter.Fig.3.13 shows the response for different value of tip mass and Fig. 3.14 shows variation for different elastic modulus.

3.3 Dynamic Analysis

Dynamic analysis of the system performed by considering different loading condition. Here time verses response of different parameter recorded.

3.3.1 Lumped parameter model Results

Lumped parameter modelling is represent in the mathematical modelling chapter here the simulation results presented as follows. Fig. 3.15 represents time verses deflection curve in sense direction for lumped model of nano vibratory beam gyroscope. Fig. 3.16 shows velocity variation with time in sense direction. Similarly Fig. 3.17 and Fig. 3.18 represents deflection and velocity variation curve in drive direction. In all Fig. the deflection is decreased with the time due to damping effect.

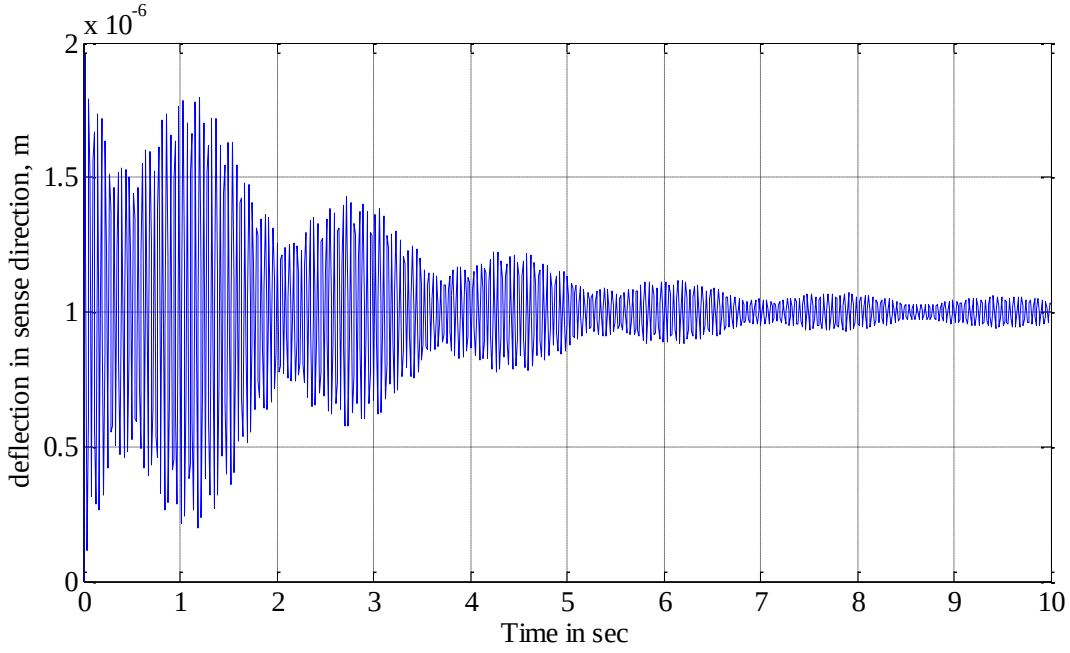

Fig. 3.15 Time v/s deflection response in Sense direction

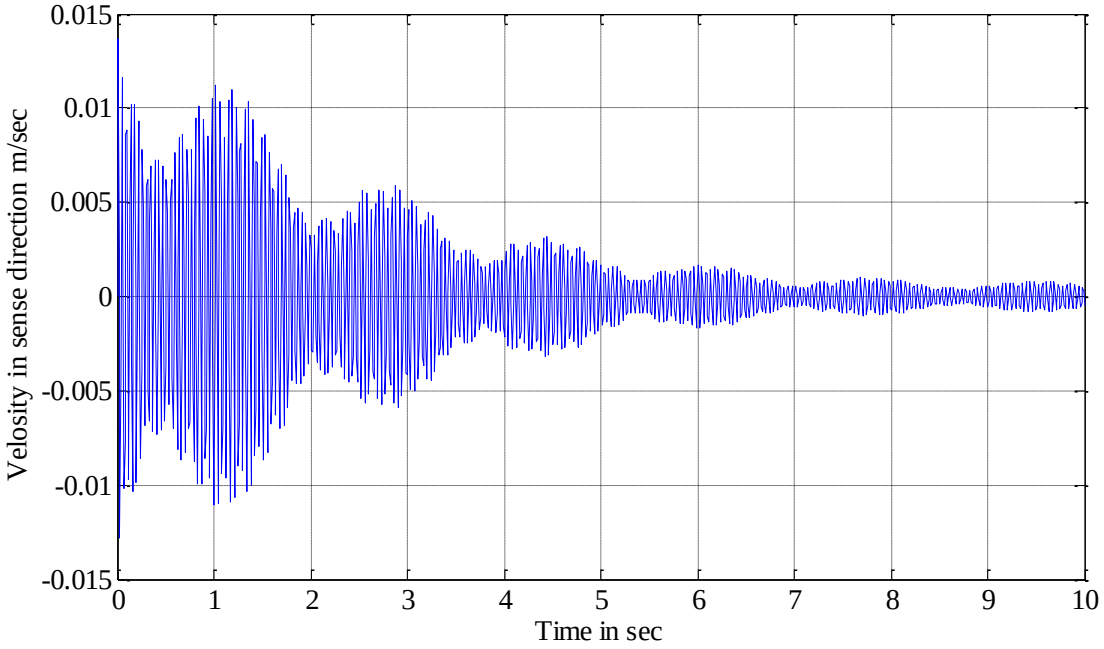

Fig. 3.16 Time v/s velocity response in Sense direction

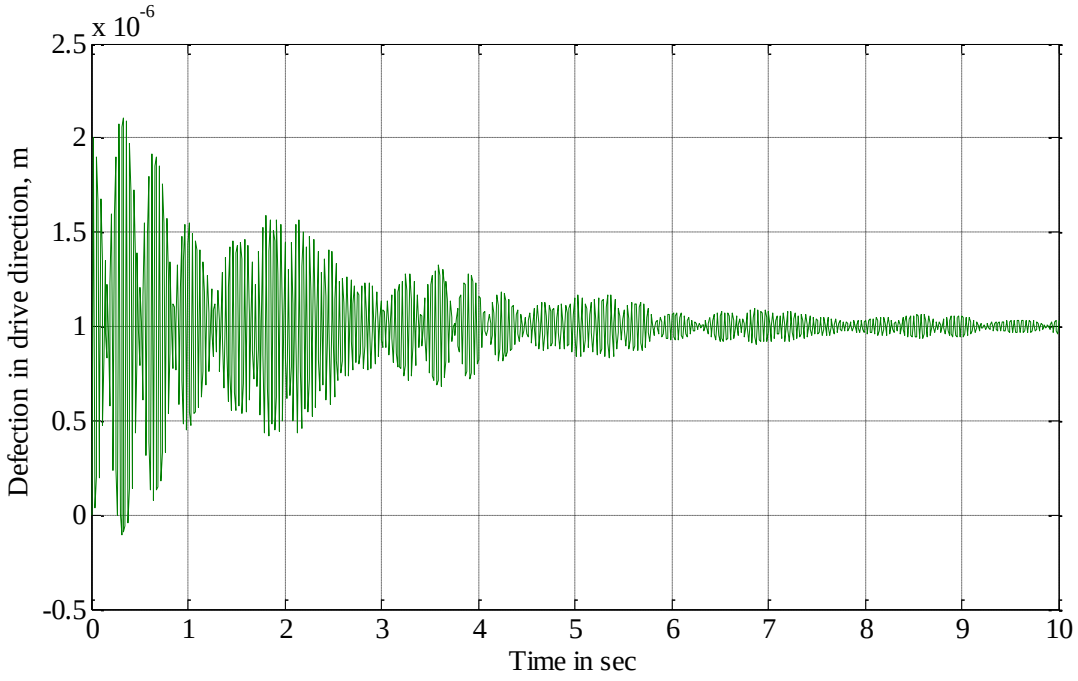

Fig. 3.17 Time v/s deflection response in Drive direction

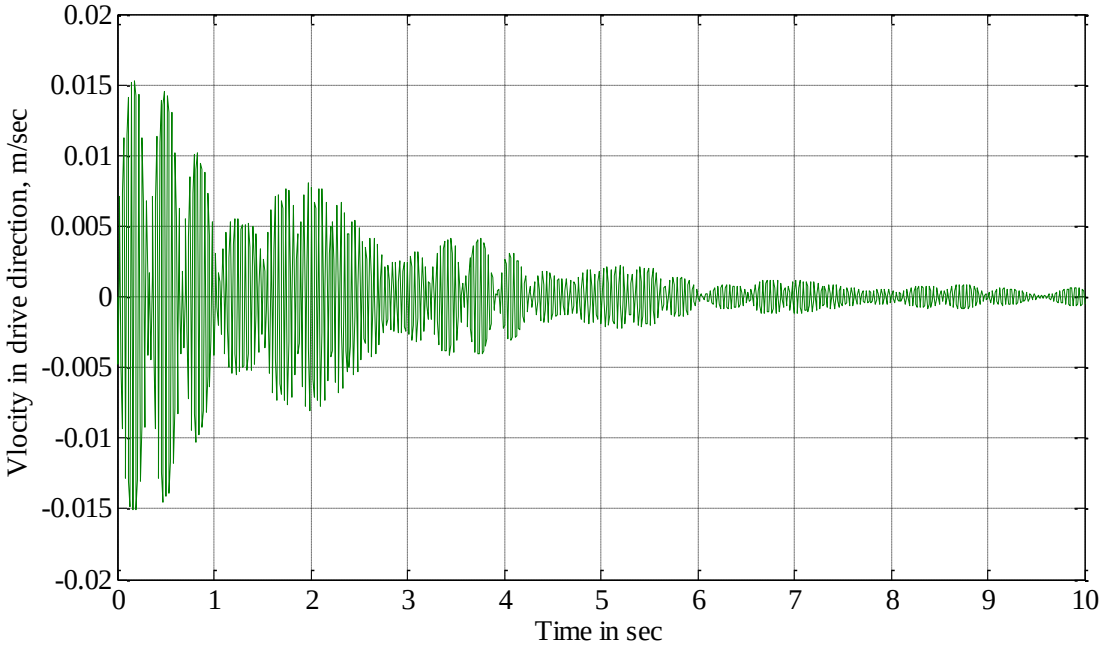

Fig. 3.18 Time v/s velocity response in Drive direction

3.3.2 Mode shape calculation

Mode shape function for the beam having tip mass is discussed in detail in 2nd chapter mathematical modelling. Fig. 3.12 represents the variation of the modal constant verses mass ratio for different mode of frequency. The mass ratio is defined as the ratio of tip mass to beam mass. The modal constant λ is the root of the frequency equation and it is solved by using Newton Raphson's solution technique. Following pseudo code is used for MATLAB simulation

```
%%%%%MAIN FUNCTION%%%%%
function y=ashish12(x)
Mr=1.0001;
y=1+cos(x)*cosh(x)+x*Mr*(cos(x)*sinh(x)-sin(x)*cosh(x));
%%%%DIFFERENTIATION OF MAIN FUNCTION%%%%
function ypr=ashish12pr(x)
Mr=1.0001;
ypr=cos(x)*sinh(x) - cosh(x)*sin(x) + Mr*(cos(x)*sinh(x) - cosh(x)*sin(x)) -
2*Mr*x*sin(x)*sinh(x);
%%%%%%%%%%%%%%%%%%%%%%%%%%%%%%%%%%%%%%%%%%%%%%%%%%%%%%%%%%%%%%%%%%%%%%%%%%%
%%%%newton raphson method for finding the root of the equation%%%%
%set tolrence
tol=0.000001;
%input initial guess
x=input ('Enter initial guess\n');
%find value of function at la
f=ashish12(x);
while abs(f)>tol
    fpr=ashish12pr(x);
    x=x-f/fpr;
    f=ashish12(x);
end
fprintf('\n\n root found: %.4f\n',x)
%%%%%%%%%%%%%%%%%%%%%%%%%%%%%%%%%%%%
```

Table 3.19 represents the modal analysis results for different mode of frequency. Here the different mass ratio taken and model constant for each value calculated and the respective frequencies are also calculated. The modal constant is inversely proportional to mass ratio and the undamped natural frequency is directly proportional to modal constant, so the mass ratio increases then the modal constant decreases and the undamped frequency of the system also decreases.

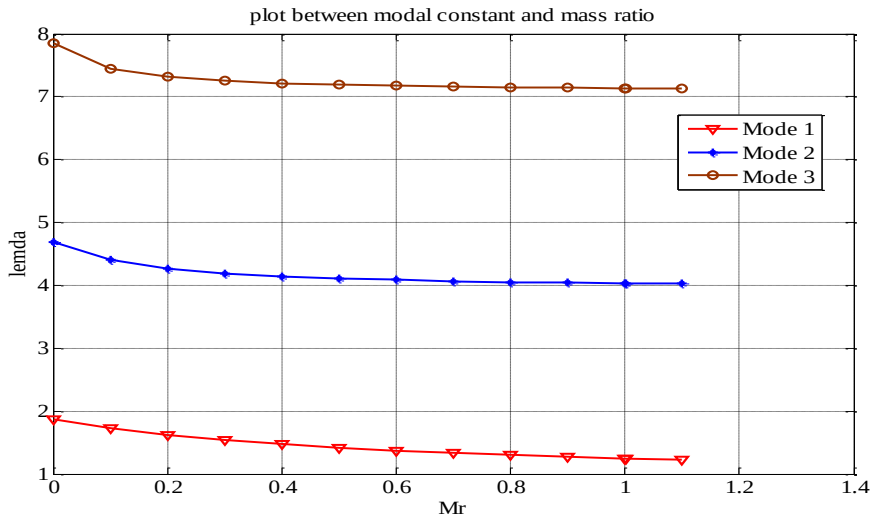

Fig. 3.19 Variation of modal constant v/s mass ratio

Table 3.4 Frequency for different value of mass ratio

S. No.	**Mass ratio** $M_r = \frac{M}{mL}$	**Modal constant, λ**			**Undamped natural frequency** $\omega = \lambda^2 \sqrt{\frac{EI}{mL^4}}$ rad/sec		
		Mode 1	Mode 2	Mode 3	Mode 1	Mode 2	Mode 3
1.	0.0	1.8751	4.6941	7.8548	148155	928479.4	2599787
2.	0.1	1.7227	4.3995	7.4511	125050.9	815594.4	2339421
3.	0.2	1.6164	4.2671	7.3184	110094.4	767243.5	2256835
4.	0.3	1.5367	4.1923	7.2537	99505.2	740580.5	2217108
5.	0.4	1.4724	4.1444	7.2155	91352.24	723753.9	2193817
6.	0.5	1.4200	4.1111	7.1903	84965.82	712170	2178520
7.	0.6	1.3757	4.0867	7.1725	79747.13	703741.4	2167748
8.	0.7	1.3375	4.0679	7.1593	75379.83	697281.5	2159776
9.	0.8	1.3041	4.0531	7.1490	71662.07	692216.9	2153566
10.	0.9	1.2745	4.0411	7.1408	68445.87	688124.1	2148628
11.	1.0	1.2479	4.0311	7.1341	65618.63	684722.7	2144598
12.	1.001	1.2477	4.0310	7.1341	65597.6	684688.7	2144598
13.	1.1	1.2239	4.0228	7.1286	63118.9	681905.9	2141293

3.3.3 Dynamic response in sense and drive direction

Dynamic response of the system recorded with the help of Galerkin's decomposition technique. For this the 4th order partial differential equations are convert into 2nd order ordinary differential equation and then runge-kutta solver is used to solve the equation in MATLAB toolbox. Following pseudo code is used for simulation.

Table 4.5 Numerical data used for damping calculation

S. No.	Parameter	Numerical value
1.	Inside gyro pressure in bar, P	101
2.	Air viscosity in Pa s, μ	18.6×10^{-6}
3.	Air mean free path in m, λ	6.71×10^{-8}

```
%%%%%FUNCTION%%%%%%
function f=prt(t,x)
f=zeros(4,1);
m=1.803e-8;Rho=2300;b=2.8*10^(-
6);J=Rho*(b^2)*(1/6);La=1.2479;M=7.2128e-12;
E=160e9;b=2.8e-6;I=(b^4)/(12);om=20;ep=8.8542e-12;Av=392e-12;Aw=392e-
12;
dv=2e-6;dw=2e-
6;wn=65597.6;g=0.01;cc=2*g*wn*M;Vdc=2;Vac=0.1*sin(314.1593*t);
a00=7.4598e6;
a1=(m-J*a00);
b1=E*I*((La)^4)-m*om^2-2*J*om^2*a00+ep*Av*Vdc^2*(dv^-3);
c1=2*m*om;
d1=ep*Av*Vdc^2*(dv^-2)*0.5*0.0155;
a2=(m-J*a00);
b2=E*I*((La)^4)-m*om^2-2*J*om^2*a00+ep*Aw*(Vdc+Vac)^2*(dw^-3);
c2=2*m*om;
d2=ep*Aw*(Vdc+Vac)^2*(dw^-2)*0.5*0.0155;
f(1)=x(2);
f(2)=((d1-b1*x(1)+c1*x(4)-cc*x(2))/a1);
f(3)=x(4);
f(4)=((d2-b2*x(3)-c2*x(2)-cc*x(4))/a2);
f=[f(1);f(2);f(3);f(4)];
%%%%%%%%%%%%%%%%%%%%%%%%%%%%
```

```
%%%%%SOLUTION%%%%%
t0=0;tf=10;c=-102.4135;x0=[0,0,0,0];
tspan=linspace(t0,tf,1000);
[t,x]=ode45('prt',tspan,x0);
plot(t,x(:,3)*c,'-r');
%%%%%%%%%%%%%%%%%%%%%%
```

3.3.3a Dynamic response without damping and inter molecular forces

Fig. 3.20 and Fig. 3.21 represents the dynamic response in sense direction without damping and inter molecular forces. Fig. 3.22 and Fig. 3.23 shows the deflection and velocity response curve in drive direction without considering the effect of damping and inter molecular forces. The amplitude of deflection and velocity increases due to absence of damping.

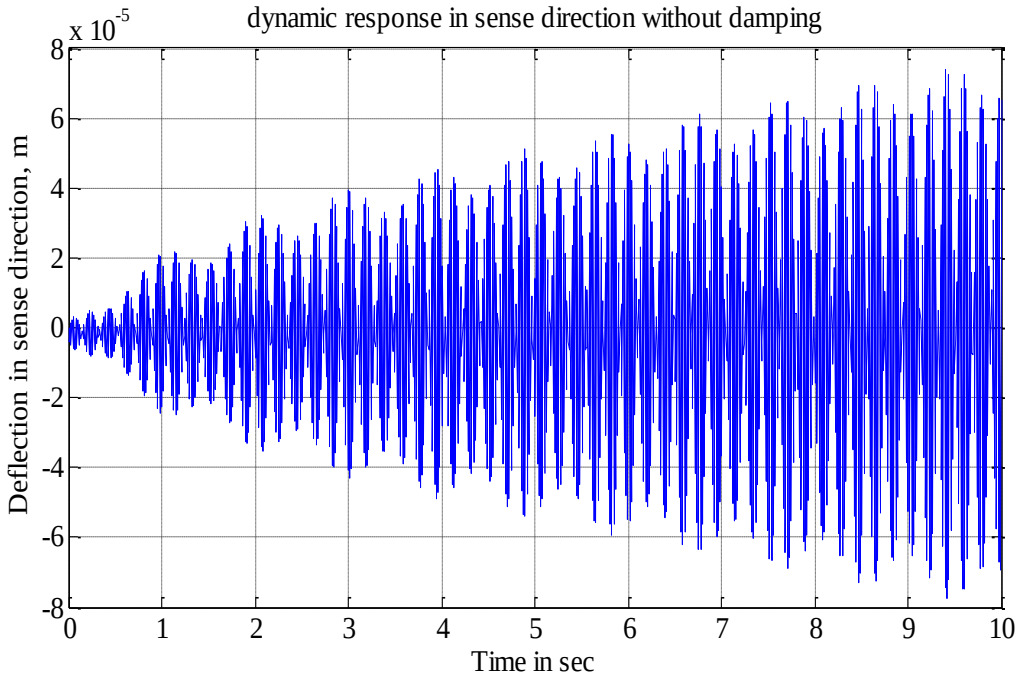

Fig. 3.20 Time verses deflection curve in sense direction without damping and inter molecular forces by using Galerkin's technique

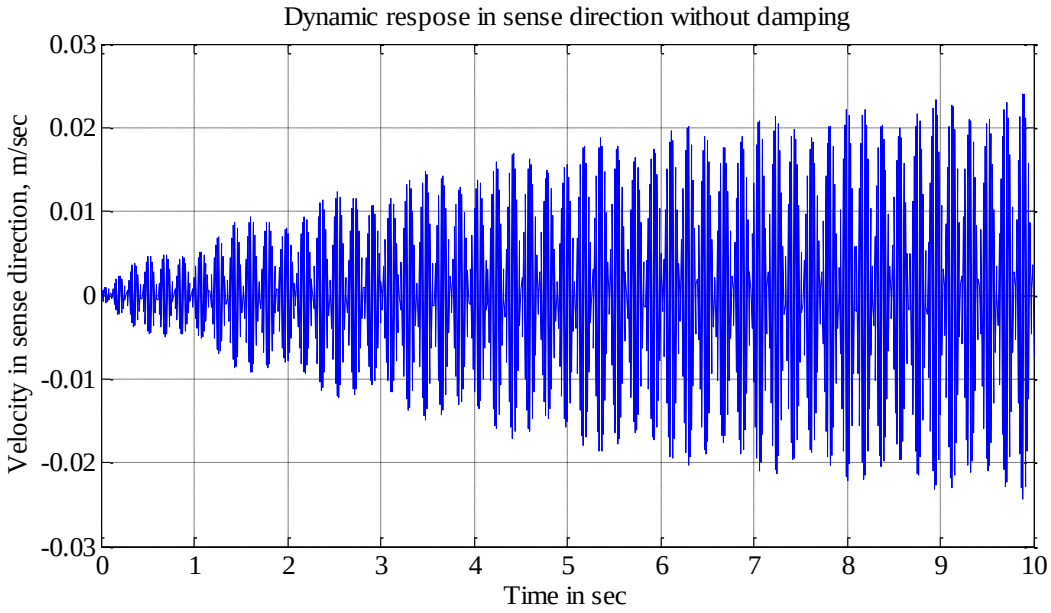

Fig. 3.21 Time verses velocity curve in sense direction without damping and inter molecular forces by using Galerkin's technique

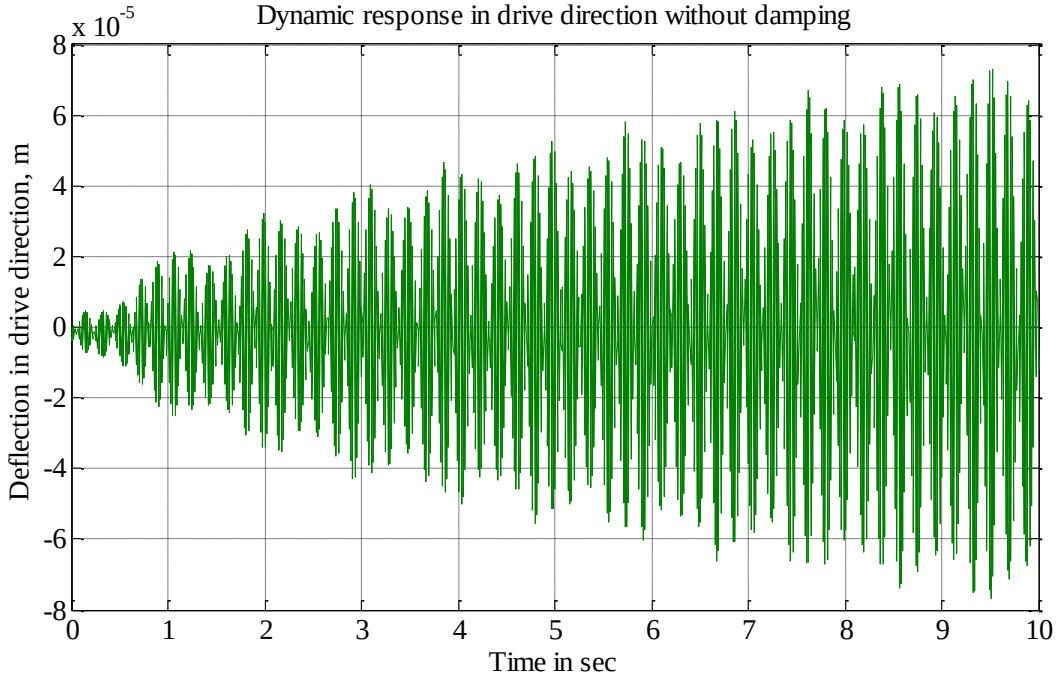

Fig. 3.22 Time verses deflection curve in drive direction without damping and inter molecular forces by using Galerkin's technique

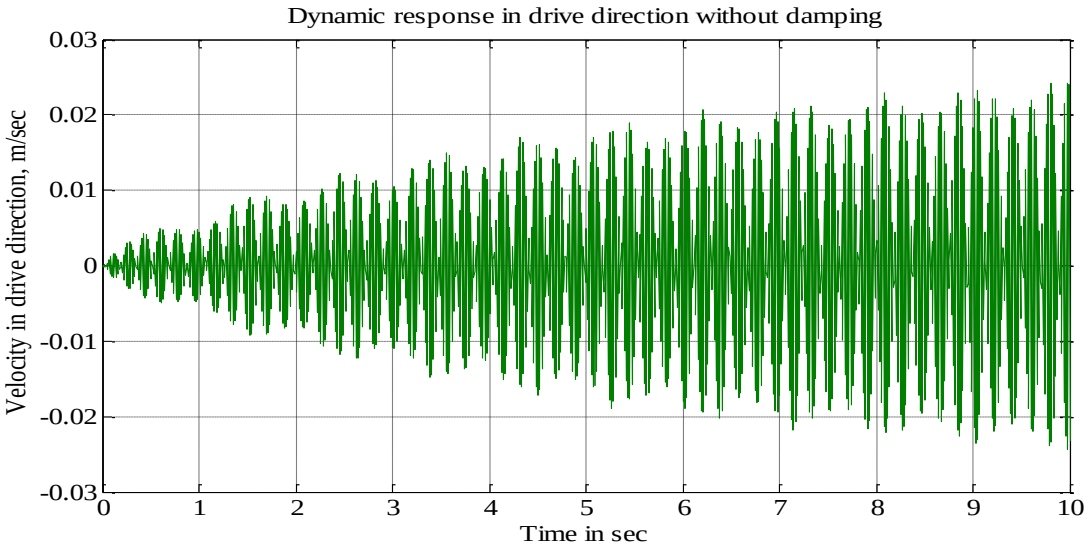

Fig. 3.23 Time verses velocity curve in drive direction without damping and inter molecular forces by using Galerkin's technique

3.3.3b Dynamic response with damping and without inter molecular forces

Fig. 3.24 and Fig. 3.25 represents the deflection and velocity curves in sense direction with consideration of damping forces and without considering the effect of inter molecular forces. The amplitude first increases then decreases in a cycle and these cycle repeated throughout the time domain and amplitude reduced due to damping.

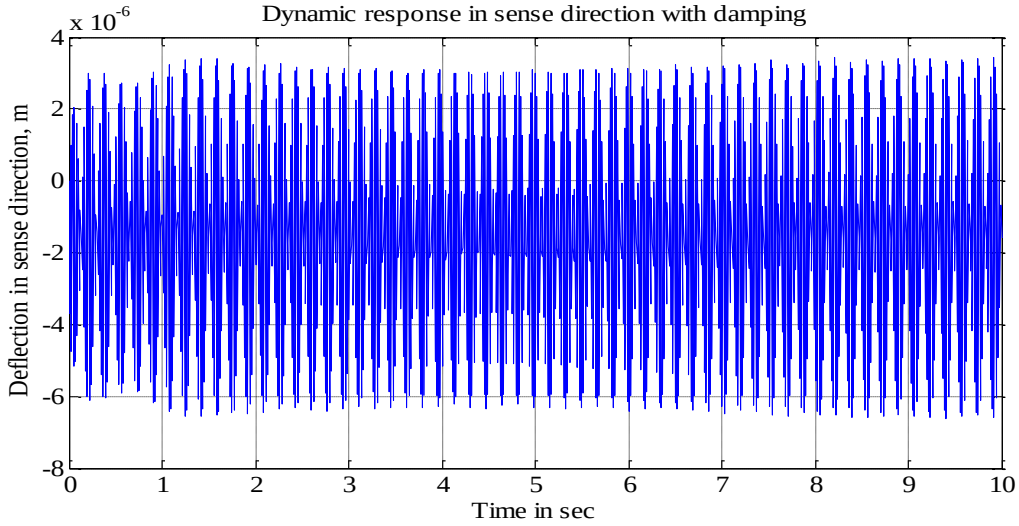

Fig. 3.24 Time verses Deflection curve in sense direction with damping and without inter molecular forces by using Galerkin's technique

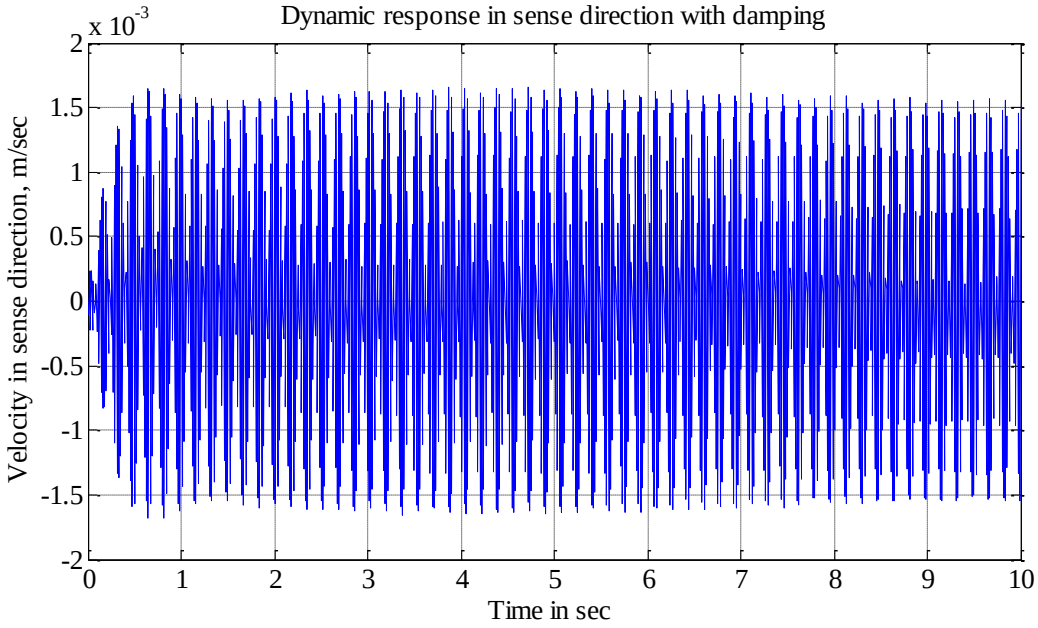

Fig. 3.25 Time verses Velocity curve in sense direction with damping and without inter molecular forces by using Galerkin's technique

Fig. 3.26 and Fig. 3.27 shows the deflection and velocity response curves in drive direction with damping effect and without inter molecular forces. It is clear from the Fig. that amplitudes have reduced due to damping.

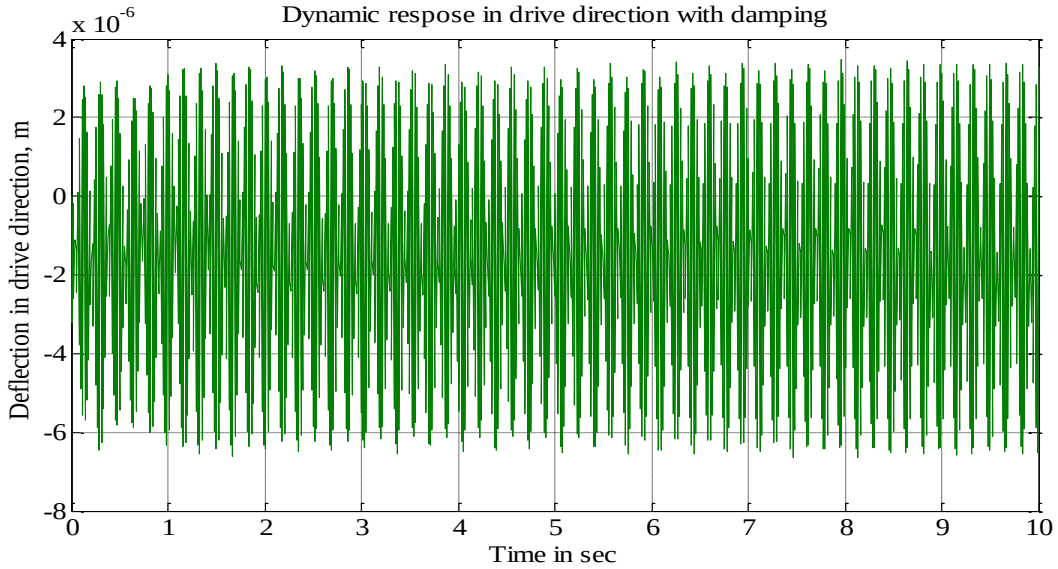

Fig. 3.26 Time verses Deflection curve in drive direction with damping and without inter molecular forces by using Galerkin's technique

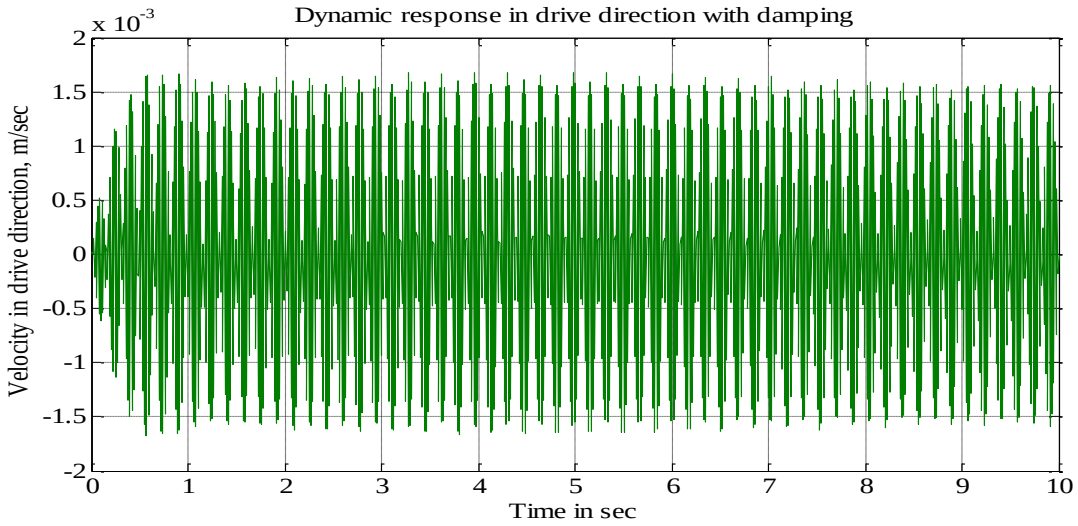

Fig. 3.27 Time verses Velocity curve in drive direction with damping and without inter molecular forces by using Galerkin's technique

3.3.3c Dynamic response with intermolecular forces and without damping

Fig. 3.28 and Fig. 3.29 represents the dynamic response in sense direction with inter molecular forces and without consideration of damping effect. The amplitude of vibration first increase and then decreases in a cycle and it increases throughout the time domain because of absence in damping.

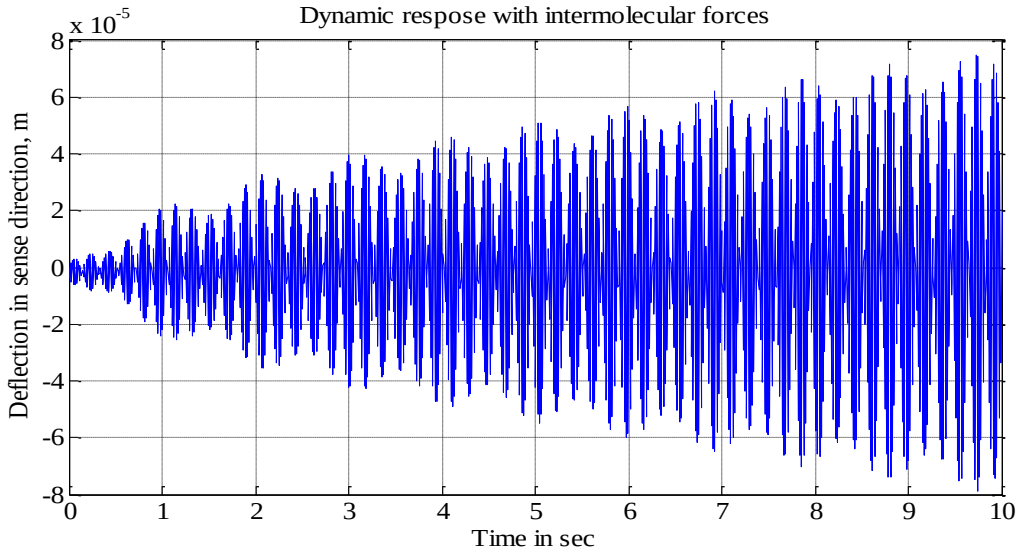

Fig. 3.28 Time verses Deflection curve in sense direction with inter molecular and without damping forces by using Galerkin's technique

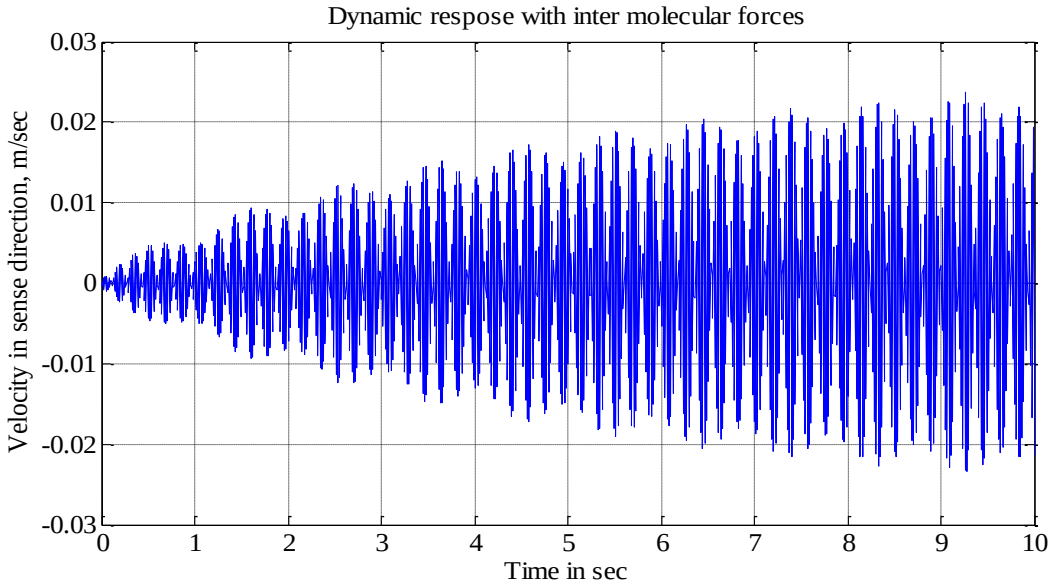

Fig. 3.29 Time verses velocity curve in sense direction with inter molecular and without damping forces by using Galerkin's technique

Fig. 3.30 and Fig. 3.31 shows the variation of deflection and velocity response by considering the effects of inter molecular forces and without damping effects. The amplitudes of vibration increasing because of absence of damping.

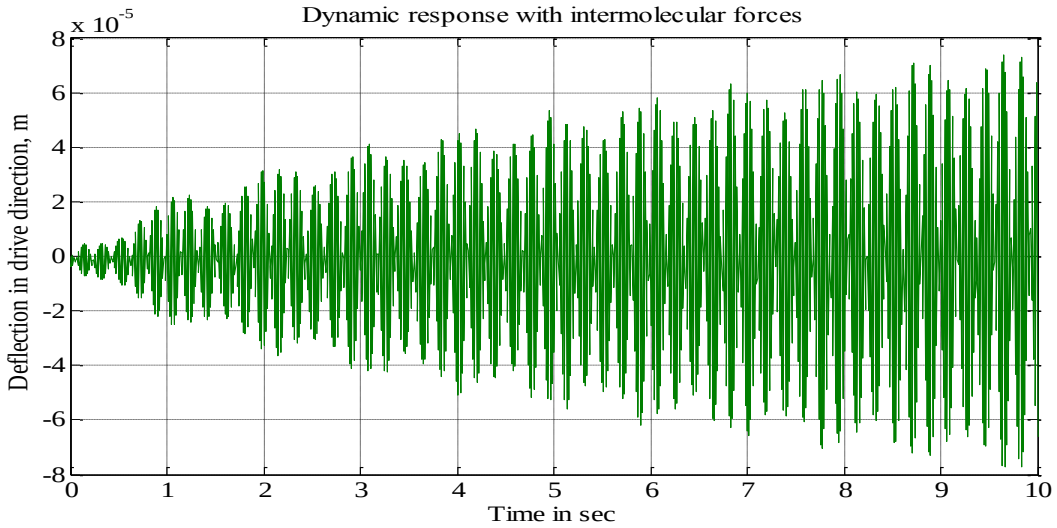

Fig. 3.30 Time verses Deflection curve in drive direction with inter molecular and without damping forces by using Galerkin's technique

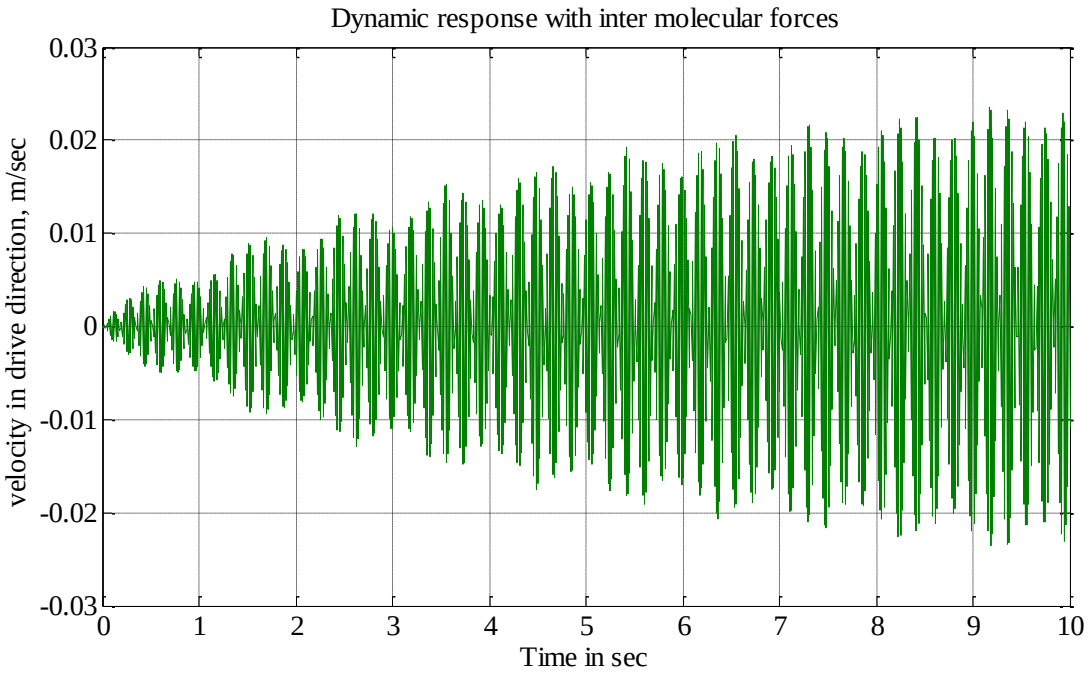

Fig. 3.31 Time verses velocity curve in drive direction with inter molecular and without damping forces by using Galerkin's technique

3.3.3d Dynamic response with damping and intermolecular forces

The effect of damping and inter molecular forces considered in the dynamic equation and the results for combined effect obtained. Fig. 3.32 and Fig. 3.33 represents the deflection and velocity response in sense direction with combined effect of damping and inter molecular forces. Similarly, Fig. 3.34 and Fig. 3.35 shows the deflection and velocity response in drive direction with the combined effect of damping and inter molecular forces. The results shows that without damping forces the amplitude of vibration increasing continuously in case of both with and without inter molecular forces, but when we consider the damping for both the cases then the amplitude of vibration first increases and after some cycle it remain constant throughout the time domain. There is significant variation observed by considering the effects of inter molecular forces. The amplitude of vibration differ for both the cases.

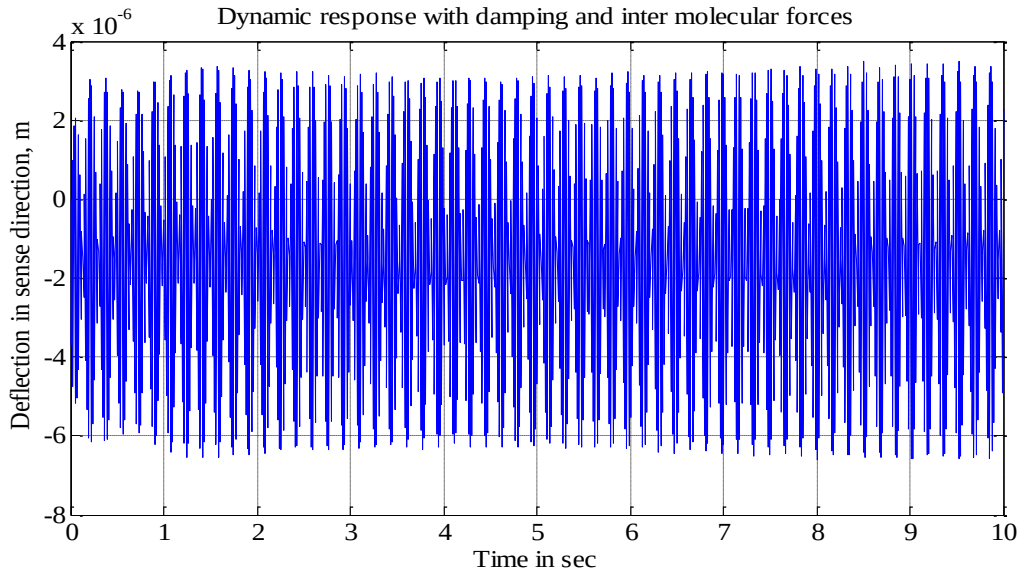

Fig. 3.32 Time verses deflection curve in sense direction with inter molecular and damping forces by using Galerkin's technique

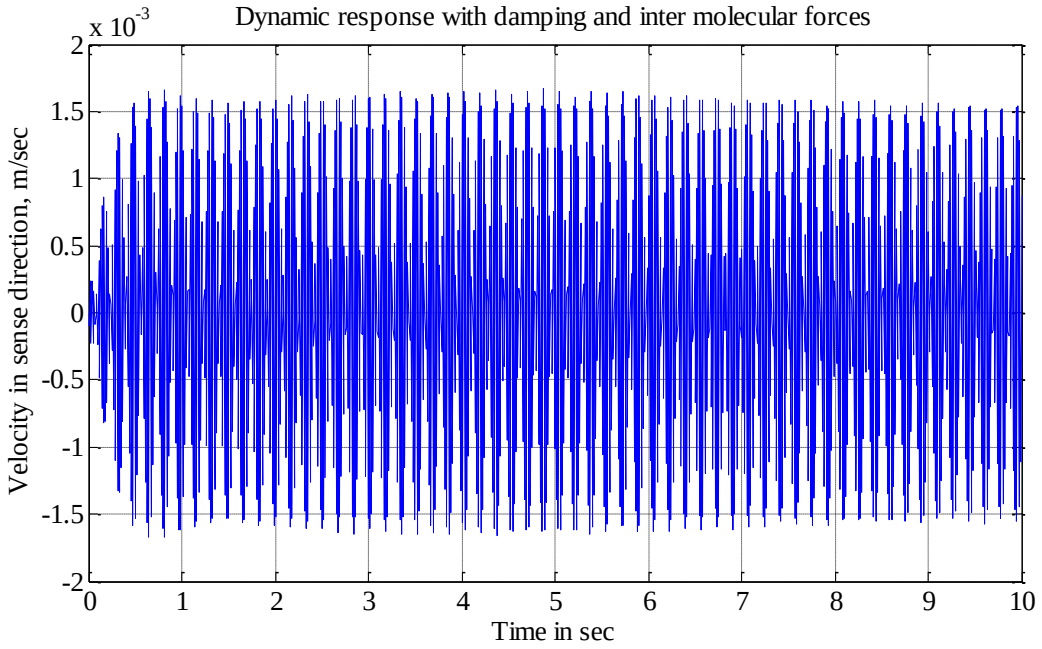

Fig. 3.33 Time verses velocity curve in sense direction with inter molecular and damping forces by using Galerkin's technique

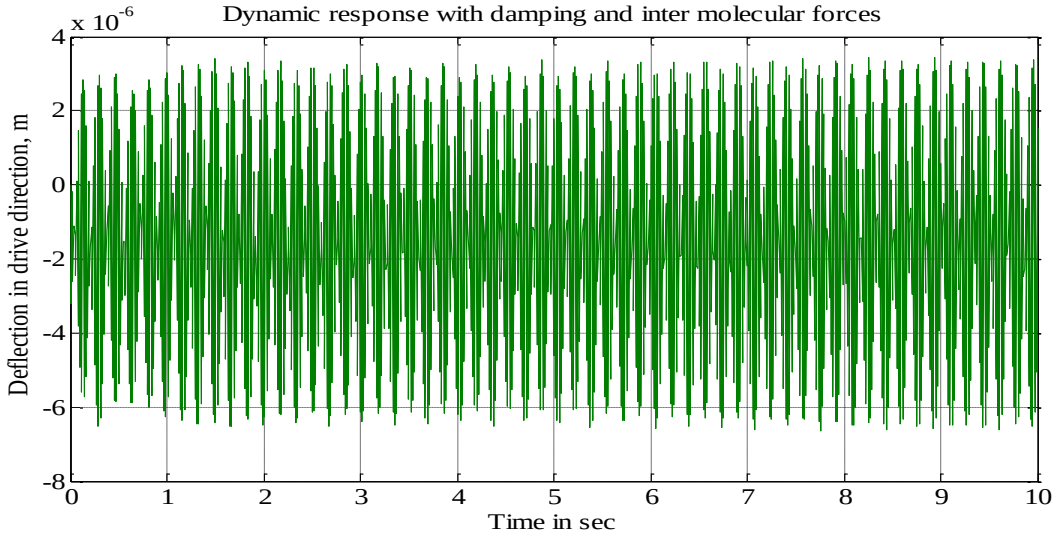

Fig. 3.34 Time verses deflection curve in drive direction with inter molecular and damping forces by using Galerkin's technique

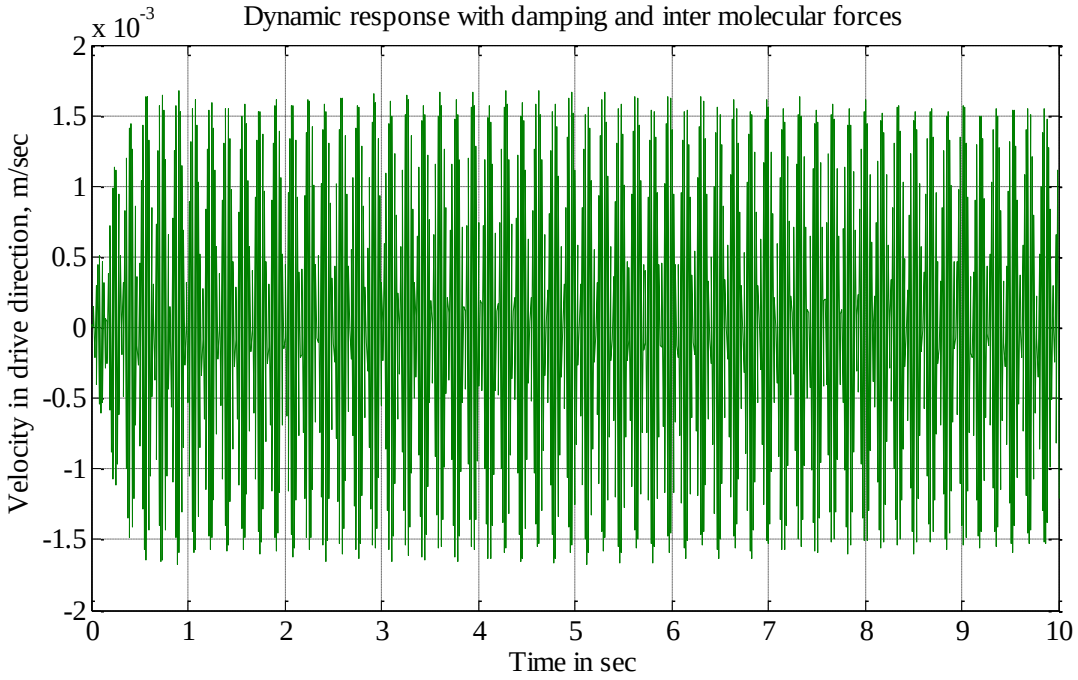

Fig. 3.35 Time verses velocity curve in drive direction with inter molecular and damping forces by using Galerkin's technique

------o------

CHAPTER 4
CONCLUSION

4.1 Summary

This work presented the design issues of nano-beam gyroscope, and its static and dynamic analysis results. The governing equations of motion were obtained by Hamilton's principle and validated from literature. The rotation of the beam was considered to be about longitudinal (x) axis, and the beam has square cross-section which is uniform throughout the length of the beam. A tip mass is attached to its end. Electrostatic sensing and actuation principles are used. The static pull-in voltage was derived at different parameter such as different rotation, different beam lengths and widths of the beam, different electrode areas, gap between the electrode and tip mass and different values of density. Inter molecular forces considered are van der waal and Casimir forces which are highly nonlinear function of displacements and the static pull-in curve drawn and the comparison made between the static pull-in behaviours of with and without inter molecular forces. Following inferences can be written:

1. Pull-in voltage decreases with increase of input angular rotation.
2. Pull-in voltage value decreases by increase in length of the beam.
3. By increasing the width of beam the pull-in voltage also increase.
4. When the area of the drive and sense electrode increases then pull-in voltage decreases.
5. Pull-in voltage increases by incrementing the gap between the tip mass and electrode.
6. With the increasing of density of the material the pull-in voltage also increases.

The natural frequency analysis also performed. The variation of the fundamental natural frequency verses applied DC voltage curves are drawn for different tip mass ratio. The dynamic analysis also carried out. The time verses deflection and velocity curves plotted for lumped parameter model of

the nano vibratory beam gyroscope for drive and sense direction. The 4^{th} order partial differential equation is reduced to 2^{nd} order ordinary differential equation with the help of Galerkin's decomposition technique and the 2^{nd} order differential equation in time variable is solved by Runge-Kutta method. The tip displacements histories were obtained by considering damping and inter molecular forces. It was found that there is a marked differences, if these forces are not considered. An attempts was made to obtain the micro cantilever sample for conducting further experiments.

4.2 Future scope

The silicon nano cantilever beam may be fabricated and the electrostatic forces can be generated by certain mechanisms. The set up can be tested using laser Doppler vibrometer for the dynamic response. Further, the results of the analysis require validation with FE method proposed in this work. Also, optimized dimensions of beam may be arrived by maximizing the sensitivity of the gyroscope. The range and resolution of this gyroscope needs to be specified by considering an electronic circuitry.

RFERENCES

[1] D. M. Shupe and J.M.O. Connor, 'Vibratory beam rotating sensor', US patent, 4, pp 381-672, 1983.

[2] K. Tanaka, Y. Mochida, M. Sugimoto, K. Moriya, T. Hasegawa, K. Atsuchi and K. Ohwada, 'A micromachined vibratory gyroscope', Sensor and actuator A, Vol. 50, pp 111-115,1995.

[3] K. Maenaka, T. Fujita, Y. Konishi and M. Maeda, 'Analysis of highly sensitive silicon gyroscope with cantilever vibrating mass', Sensor and actuator A, Vol. 54, pp 568-573, 1996.

[4] Katz and A. Highsmith, 'The optimal size of a resonant vibrating beam Gyroscope', Journal of Dynamic Systems, Measurement, and Control Vol. 123, pp 49–54, 2001.

[5] J. Yang and H. Fang, 'Analysis of a Rotating Elastic Beam with Piezoelectric Films as an Angular Rate Sensor', IEEE Transactions on Ultrasonics, ferroelectrics, and frequency control, Vol. 49, pp 798-804, 2002.

[6] S. Kausinis and R. Barauskas, 'Computer simulation of piezoelectric angular rate sensor', Measurement, vol. 39, pp.947-958, 2006.

[7] Qingkai Yu, Guoting Qin, Chinmay Darne, Chengzhi Cai , Wanda Wosik and Shin Shem Pei, 'Fabrication of short and thin silicon cantilevers for AFM with SOI wafers', Sensors and Actuators, Vol. 126, pp 369–374, 2006.

[8] J.Seoka and H. Scarton, 'Dynamic characteristics of a beam angular-rate sensor', International Journal of Mechanical Sciences, Vol. 48, pp. 11–20, 2006.

[9] M. Esmaeili, N. Jalilib and M. Durali, 'Dynamic modeling and performance evaluation of a vibrating beam microgyroscope under general support motion', Journal of Sound and Vibration Vol. 301, pp. 146-164, 2007.

[10] F. Asokanthan, and J. Cho, 'Dynamic Stability of Beam-type Vibratory Angular Rate Sensors Subjected to Rate Fluctuations', J. Int.Material systems and Structures, Vol. 19, pp. 735- 743, 2008.

[11] V. Bhadbhade, N. Jalili and S. Mahmoodi, 'A novel piezoelectrically actuated flexural/torsional Vibrating beam gyroscope', Journal of Sound and Vibration, Vol. 311, pp. 1305–1324, 2008.

[12] M. Ghommem, A. Nayfeh, S. Choura, F. Najar and E. Abdel-Rahman, **'**Modeling and performance study of a beam microgyroscope', Sound and Vibration, Vol. 329, pp. 4970-4979, 2010.

[13] Z. Hou, D. Xiao, X. Wu, P. Dong, Z. Chen, Z. Niu and X. Zhang, 'Effect of Axial Force on the Performance of Micromachined Vibratory Rate Gyroscopes', Sensors Vol. 11, pp 296-309, 2011.

[14] M. Rasekh and S. Khadem, 'Design and performance analysis of a Nano-gyroscope based on electrostatic actuation and capacitive sensing', Sound and Vibration, Vol.332, pp.6155-6168, 2013.

[15] S. Lajimi, G. Heppler and E. Rahman, 'A new cantilever beam-rigid-body MEMS gyroscope, mathematical model and linear dynamics', Proceedings of the International Conference on Mechanical Engineering and Mechatronics Toronto, Ontario, Canada, pp XXX1-XXX6, 2013.

[16] S. Lajimi, G. Heppler and E. Rahman, 'Eigenvalue analysis of a cantilever beam rigid body MEMS gyroscope', Proceedings of the International Conference on Mechanical Engineering and Mechatronics Toronto, Ontario, Canada, pp. XXX1-XXX5, 2013.

[17] W. Wang, X. Lu and D. Xu, 'Design of multi degree of freedom micromachined vibratory gyroscope with double sense mode', Measurement, vol. 58, pp. 6-11, 2014.

[18] A. Moghaddam and M. Zand, 'Effect of design parameters on pull-in and vibration of microbeam gyroscope', 4th International conference on acoustics & vibration (ISAV2014), Tehran, Iran, 2014.

[19] M. Mojahedi, M. Ahmadian and K. Firoozbakhsh, 'The influence of the intermolecular surface forces on the static deflection and pull-in instability of the micro / nano cantilever gyroscope', Composites Part B: Engineering, vol. 56, pp 336-343, 2014.

[20] M.M. Zand and A.O. Moghaddam, 'Pull-in instability and vibration of microgyroscope', JAMECH, Vol. 45, pp 29-34, 2014.

[21] A. Burg, A. Meruani, B. Sandheinrich and M. Wickmann, 'MEMS gyroscope and their application', ME-381, introduction to micro-electro-mechanical system. (http://clifton.mech.northwestern.edu/~me381/project/done/Gyroscope.pdf).

[22] K. S. Elliott, P. Gupta, K. B. Reed and R. C. Rodriguez, 'project report on Micromachined vibrating gyroscopes, Design and fabrication', North-western University.

APPENDIX

RUNGE-KUTTA SOLUTION FOR TIME INTEGRATION

Consider set of n-simultaneous ordinary diff. eqs in canonical form:

$$\frac{dy_1}{dt} = f_1(t, y_1, y_2, ...y_n)$$

$$\frac{dy_2}{dt} = f_2(t, y_1, y_2, ...y_n)$$

$$\frac{dy_n}{dt} = f_n(t, y_1, y_2, ...y_n)$$

By expanding using 4th order R-K formulas we get,

$$y_{i+1,j} = y_i + \frac{1}{6}(k_{1j} + 2k_{2j} + 3k_{3j} + 4k_{4j}) + O(h^5);\ j = 1,2,3,.....n$$

$$k_{1j} = hf_j(t_i, y_{i1}, y_{i2}, ...y_{in})$$

$$k_{2j} = hf_j(t_i + \frac{h}{2}, y_{i1} + \frac{k_{11}}{2}, y_{i2} + \frac{k_{12}}{2}, ...y_{in} + \frac{k_{1n}}{2})$$

$$k_{3j} = hf_j(t_i + \frac{h}{2}, y_{i1} + \frac{k_{21}}{2}, y_{i2} + \frac{k_{22}}{2}, ...y_{in} + \frac{k_{2n}}{2})$$

$$k_{4j} = hf_j(t_i + h, y_{i1} + \frac{k_{31}}{2}, y_{i2} + \frac{k_{32}}{2}, ...y_{in} + \frac{k_{3n}}{2})$$

This method is programmable using nested loops.

In MATLAB, the values of *k, y* can be put into vectors to easily evaluate in matrix form.

Following pseudo code is adopted in this work:

```
%%%%%%%%%%%%%%%%%%%%%%%%%%%%%%%%%%%%%%%%%%%%%%%%%%%%%%%%%%%%%%%%%%%%%%%%
x01=0;x02=0;
r=0.5;pe=1000;
h=2*pi/r/pe;
tma=700;
i=1;
for t0=0:h:tma
X1(i)=x01;X2(i)=x02;
k1=h*g1(x01,x02,t0); l1=h*g2(x01,x02,t0);
k2=h*g1(x01+0.5*k1,x02+0.5*l1,t0+h/2);
l2=h*g2(x01+0.5*k1,x02+0.5*l1,t0+h/2);
k3=h*g1(x01+0.5*k2,x02+0.5*l2,t0+h/2);
l3=h*g2(x01+0.5*k2,x02+0.5*l2,t0+h/2);
```

```
k4=h*g1(x01+k3,x02+l3,t0+h); l4=h*g2(x01+k3,x02+l3,t0+h);
x1n=x01+(k1+2*k2+2*k3+k4)/6; x2n=x02+(l1+2*l2+2*l3+l4)/6;
x01=x1n;
x02=x2n;
i=i+1;
end
% Generation of x1(nt) and x2(nt)
T=[0:h:tma];
for j=2*pe:pe:length(T)
n=(j-pe)/pe;
X3(n)=X1(n*pe);
X4(n)=X2(n*pe);
end
%%%%%%%%%%%%%%%%%%%%%%%%%%%%%%%%%%%%%%%%%%%%
```